RESEARCH AND DEVELOPMENT TECHNICAL REPORT
ECOM-5558

ATMOSPHERIC EFFECTS FOR GROUND TARGET SIGNATURE MODELING

III. Discussion and Application of the ASL Scattering Model

By

Richard B. Gomez

Carmine Petracca

Charles Querfeld

Glenn B. Hoidale

Atmospheric Sciences Laboratory

US Army Electronics Command .
White Sands Missile Range, New Mexico 88002

20081121 353

March 1975

Approved for public release; distribution unlimited.

ECOM

UNITED STATES ARMY ELECTRONICS COMMAND - FORT MONMOUTH, NEW JERSEY 07703

NOTICES

REPORT DOCUMENTATION PAGE		READ INSTRUCTIONS BEFORE COMPLETING FORM
1. REPORT NUMBER ECOM-5558	2. GOVT ACCESSION NO.	3. RECIPIENT'S CATALOG NUMBER
4. TITLE *(and Subtitle)* ATMOSPHERIC EFFECTS FOR GROUND TARGET SIGNATURE MODELING III. Discussion and Application of the ASL Scattering Model		5. TYPE OF REPORT & PERIOD COVERED
		6. PERFORMING ORG. REPORT NUMBER
7. AUTHOR(s) Richard B. Gomez, Carmine Petracca, Charles Querfeld, and Glenn B. Hoidale		8. CONTRACT OR GRANT NUMBER(s)
9. PERFORMING ORGANIZATION NAME AND ADDRESS Atmospheric Sciences Laboratory White Sands Missile Range, New Mexico 88002		10. PROGRAM ELEMENT, PROJECT, TASK AREA & WORK UNIT NUMBERS DA Task No. 1T161102B53A-19
11. CONTROLLING OFFICE NAME AND ADDRESS US Army Electronics Command Fort Monmouth, New Jersey 07703		12. REPORT DATE March 1975
		13. NUMBER OF PAGES 34
14. MONITORING AGENCY NAME & ADDRESS*(if different from Controlling Office)*		15. SECURITY CLASS. *(of this report)* Unclassified
		15a. DECLASSIFICATION/DOWNGRADING SCHEDULE

16. DISTRIBUTION STATEMENT *(of this Report)*

Approved for public release; distribution unlimited.

17. DISTRIBUTION STATEMENT *(of the abstract entered in Block 20, if different from Report)*

18. SUPPLEMENTARY NOTES

Dr. Querfeld is Staff Scientist at the High Altitude Observatory, National Center for Atmospheric Research, Boulder, Colorado.

19. KEY WORDS *(Continue on reverse side if necessary and identify by block number)*

1. atmospheric optics   5. atmospheric aerosol
2. radiative transfer
3. scattering
4. low visibility

20. ABSTRACT *(Continue on reverse side if necessary and identify by block number)*

This report describes the Atmospheric Sciences Laboratory's single scattering model, which was developed for input to multiple scattering codes for the determination of electromagnetic extinction caused by the atmospheric aerosol. Sample applications of the model are made to the cases of haze and dust. In addition, the role that the scattering model plays in the overall radiative transfer problem is described.

DD FORM 1473 1 JAN 73   EDITION OF 1 NOV 65 IS OBSOLETE

INTRODUCTION

This is the third in a series of reports [1-2] prepared in support of
the atmospheric modeling portion of the Army Materiel Command's Target
Signature Analysis (TSA) program (formerly called the Ground Target
Signature Program). The aim of the atmospheric modeling project is
to predict absorption and scattering effects of the atmospheric medium
on the transmission of ground target electromagnetic (EM) signatures
in the spectral region 0.4-14 μm, for a wide range of meteorological
conditions. Special attention is being given to low visibility atmos-
pheric states which can exist under battlefield conditions.

Two important related aspects of the program are the atmospheric ex-
tinction and radiative transfer models. These models will be integrated
into system performance models for the evaluation of terminal homing,
surveillance, and target acquisition systems. Previous reports [1-2]
have described atmospheric transmission at 1.06 μm and have presented a
generalized method for the determination of EM attenuation due to the
process of molecular absorption. This report will describe the Atmos-
pheric Sciences Laboratory's (ASL) single scattering model, which was
developed for input to multiple scattering codes for the determination
of EM extinction caused by the atmospheric aerosol. These multiple
scattering codes will be described in a separate report. Sample
applications will be made to the cases of haze and dust. In addition,
the role that the ASL single scattering model plays in the overall
radiative transfer problem will be described.

In the remainder of this paper, in addition to the description of the
ASL single scattering model, the following topics are considered:
a discussion of the physical and optical characteristics of the atmos-
pheric aerosol relevant to any application of the model; the versatility
of the ASL model through its application to the atmospheric conditions
of haze and dust; and the role that the ASL model plays in the overall
radiative transfer problem. The theoretical basis of the ASL scattering
model is given in the Appendix.

THE ASL SCATTERING MODEL

In the spectral region of interest (0.4-14 μm) the scattering of electro-
magnetic energy (EM) by the atmospheric gases is well known and will not
be further discussed. The scattering coefficient for a Rayleigh atmosphere
can be easily calculated [3]. The question of EM extinction by aerosols

is an entirely different matter, however, because of the aerosols' complexity. The ASL single scattering model is a first step in addressing the aerosol problem. It utilizes the Mie scattering theory together with various size distribution options to compute the necessary parameters for input to multiple scattering codes for application to low visibility atmospheric conditions. The main parameters of interest computed with the ASL model are the extinction, scattering, and absorption cross sections, the single scattering albedo, and the single scattering phase function.

In the context of this report the atmospheric aerosol is understood to be a colloidal system in which the dispersed phase is composed of suspended and precipitating solid and liquid particles, and the dispersive medium is air. We are primarily concerned in the long run with aerosols in which the dispersed phase (solid or liquid particles) gives rise to low visibilities in the atmosphere; i.e., when the visibility is 11 km or less.

In order to define unambiguously the state of aerosols in the atmosphere, one must specify the following: (1) size distribution, (2) number density, (3) composition, (4) shape, and (5) spatial and temporal distribution.

The size distribution is an important factor and defines certain types of atmospheres. The size distribution for hazes is quite different from that for fogs and clouds, with the peak of the distribution lying in the region of smaller sized particles. A variety of distribution functions such as the Junge, modified gamma, and the log-normal can be used to model a particular state. The distribution function n depends on the size of the particles and the altitude; i.e.,

$$n = n(z, r), \qquad (1)$$

and represents the particle partial number density per unit increment of the particle radius r at an altitude z. The total number density N at altitude z is given by

$$N(z) = \int_{r_m}^{r_M} n(z, r) \, dr, \qquad (2)$$

where r_m and r_M are the minimum and maximum radii of the distribution.

Determining the composition of aerosols is a more difficult procedure. One doesn't necessarily need the exact chemical composition but rather the optical properties of the aerosols, such as the real and imaginary parts of the refractive index. Samples of the atmosphere can be taken from various geographical areas and experiments performed to determine the bulk complex refractive index. It is especially important that the

imaginary part of the refractive index be determined, since results of calculations show that the radiation field is quite sensitive to that component [4].

The shape of particulates in the atmosphere is very difficult to estimate. For liquid aerosols one can usually assume the shape to be spherical, but for the dry dust aerosols the shape may be quite irregular. How the shape affects the optical properties of a distribution of particles is not well known, although it is known that the scattering properties are different from those of a spherical particle [5]. Much more theoretical and experimental research on this problem is needed. In this report, all particles, liquid or solid, are assumed to be spherical.

Finally, the spatial and temporal distributions of aerosols are needed to define unambiguously the atmospheric state. It is usually assumed that the vertical distribution of particle number density does not vary in time and is a monotonically decreasing function of altitude, and sometimes an exponential decrease of particle concentration in the size range from 10^{-2} to 1 μm up to a height of 4-6 km is used; i.e.,

$$N(z) = N(o)e^{-z/H}, \tag{3}$$

where $N(z)$ and $N(o)$ are the particle concentrations at heights z and ground level, respectively. H is an empirical constant that varies with location. More modeling efforts are needed to define the vertical distribution and its change in time for various hazes, fogs, clouds, dust, smokes, etc. Most radiative transfer models assume a horizontally homogeneous atmosphere - one in which the optical properties do not vary within a horizontal plane. In some cases, especially in a highly localized military setting, this is probably a poor assumption.

How does a knowledge of aerosols aid in radiation studies? In the following ways: In order to determine the aerosol optical depth τ between points z_1 and z_2, one needs the volume extinction coefficient $\gamma_{ext}(z)$:

$$\tau = \int_{z_1}^{z_2} \gamma_{ext}(z)dz, \ z_1 < z < z_2 . \tag{4}$$

The volume extinction coefficient $\gamma_{ext}(z)$ in turn depends on the total number density $N(z)$ and the total extinction cross section C_{ext}:

$$\gamma_{ext}(z) = N(z)C_{ext}, \tag{5}$$

3

where the effective total extinction cross section C_{ext} is given by

$$C_{ext} = \int_{r_m}^{r_M} C_{ext}(r) \, n(r) dr \quad ; \qquad \int_{r_m}^{r_M} n(r) dr = 1 \qquad (6)$$

in which $n(r)$ is the size distribution function for spherical particles of identical optical properties, $C_{ext}(r)$ is the extinction cross section, and the size distribution has been normalized to unity. The ASL scattering model will allow C_{ext} to be calculated for variable complex refractive index $m(\lambda)$ and size distribution $n(r)$. Here λ is the wavelength of the incident radiation. The model can also be used to calculate the single scattering phase functions for any size distribution and complex refractive index.

In addition, the ASL scattering model can be used to calculate the scattering cross section C_{sca} and therefore determine $\beta_{sca}(z)$, the volume scattering coefficient. Thus, the single-scattering albedo ω_o can be calculated:

$$\omega_o = \frac{\beta_{sca}(z)}{\gamma_{ext}(z)} = \frac{C_{sca}}{C_{ext}} = \frac{C_{sca}}{C_{sca} + C_{abs}} \, . \qquad (7)$$

The difference of the extinction and scattering cross sections is the absorption cross section C_{abs} which can be used to calculate the absorption coefficient α_{abs}.

In order to do more than a simple parametric study of the natural radiation field in the atmosphere by arbitrarily varying the optical properties, one needs realistic estimates of the optical depth and the scattering phase function. These in turn require realistic descriptions and estimates of the kinds and quantities of particulates in the atmosphere. Since the natural atmospheric aerosol consists of both liquid drops and irregular fragments of solid materials, the theoretical prediction of the scattering properties of the natural aerosol has a number of severe limitations which stem from the usual lack of information concerning the complex refractive index of the particles, their internal homogeneity and isotropy, and their size, shape, orientation and number density. In view of these uncertainties, it is normal to assume that all aerosol constituents are spherical and isotropic, and that size, number density, and bulk optical properties may be measured or assumed. The reason for this is that rigorous scattering theory for nonspherical scatterers is extremely complex. Consequently, the ASL scattering model employs the well-known Mie theory of scattering by spherical particles of arbitrary size. Elements of Mie theory necessary for an understanding of the numerical algorithms used in the ASL model are discussed in the Appendix.

Aerosols are generally described for Mie computations by their complex refractive index, particle size distribution, and number density. A useful approach in analyzing the impact of these complex and highly variable factors on the transmission of EM energy is to adopt typical or average values for these parameters of the dispersed phase for a representative set of meteorological conditions and to then adjust these values as required for other conditions.

We have adopted five different options for describing the particle size distribution: an arbitrary one, log-normal, Junge [6], Deirmendjian model C [7], and generalized Khrgian and Mazin [8, 9]. The best known distribution function - the normal or Gaussian - was not adopted here because it is symmetrical and is calculated under the assumption that negative particle radii can occur.

The arbitrary distribution allows the input of tabulated distributions. The radius r and its associated frequency of occurrence n(r) are simply read. This may be useful in comparing results between experimentally measured distributions and theoretical, functional ones.

The log-normal distribution which has been adopted does not admit negative values of particle radii, but it does show the skewness of naturally occurring aerosol particle populations. In the case of the log-normal distribution, it is $x = \ln r$ rather than r which is normally distributed, with mean value $\bar{x}$ and dispersion σ^2_x. That is,

$$n(r)dr = \left\{ \frac{1}{\sigma_x\sqrt{2\pi}} \exp \left[- \frac{(x-\bar{x})^2}{2\sigma^2_x} \right] \right\} dx, \tag{8}$$

but $dx = d(\ln r) = \frac{dr}{r}$, so that

$$n(r) = \frac{1}{r\sigma_x\sqrt{2\pi}} \exp \left[- \frac{(x-\bar{x})^2}{2\sigma^2_x} \right], \tag{9}$$

where

$$\bar{x} = \int_{r_m}^{r_M} (\ln r)n(r)dr \tag{10}$$

and

$$\sigma^2_x = \int_{r_m}^{r_M} (\ln r-\bar{x})^2 n(r)dr. \tag{11}$$

5

The mean value $\bar{x}$ is usually written in terms of the geometric mean value r_g as follows:

$$\bar{x} = \frac{1}{N} \sum_{i=1}^{N} \ln r_i = \ln \left(\prod_{i=1}^{N} r_i \right)^{1/N} = \ln r_g. \tag{12}$$

In addition, the standard deviation σ_x is usually written in terms of the geometric mean standard deviation σ_g as follows:

$$\sigma_x = \ln \sigma_g. \tag{13}$$

Hence, one can calculate the frequency of occurrence of particles with radius r by the relation

$$n(r) = \frac{1}{r \ln \sigma_g \sqrt{2\pi}} \exp \left\{ -\frac{1}{2} \left[\frac{\ln(r/r_g)}{\ln \sigma_g} \right]^2 \right\}. \tag{14}$$

This distribution has been found to describe stratus cloud droplets, rock dust formed by mechanical grinding, mists produced by a disk atomizer, and coalescent aerosols of NH_4Cl and H_2SO_4 formed by mixing gaseous reagents [10].

The Junge distribution is given by

$$n(r) = Cr^{-\beta}, \tag{15}$$

where C and β are constants. This distribution is used widely to describe natural aerosols such as mists and dusts, and is generally accepted as valid for 0.1 μm<r<15 μm. For smaller particles, a constant frequency of occurrence is generally used:

$$n(r) = C^1. \tag{16}$$

The constant β in Eq. (15) ranges between 2 and 5 for natural aerosols, depending upon the total particle concentration. The constant C in Eq. (15) may be determined by integrating Eq. (15) over its size distribution range and equating the result to experimentally determined number concentrations. Work done at White Sands Missile Range, NM, by Henley and Hoidale [11] indicate that for dust C may vary from 0.3 to 30 cm^{-3}, corresponding to low and high dust concentrations, respectively. In a similar way the constant C^1 in Eq. (16) can also be determined. Henley and Hoidale [11] found that for dust C^1 varies from 10^3 to $10^5 cm^{-3}$ for low to high dust concentrations. In the specific dust distribution example discussed in the next section, we have chosen to use the distributions Eq. (15) and Eq. (16) with $\beta = 4$, C = 30 cm^{-3}, and $C^1 = 10^5 cm^{-3}$. This corresponds to a high dust concentration and therefore to low visibility.

6

The Deirmendjian model C haze is a modified Junge distribution. Since it too has found wide application to continental hazes, we have included it in our model. The actual distribution used is

$$
\begin{aligned}
n(r) &= 0 & r &< 0.03\mu m \\
n(r) &= 2.251 \times 10^4 & 0.03\mu m &\leq r \leq 0.1\mu m \\
n(r) &= 2.251 r^{-4} & 0.1\mu m &< r \leq \infty.
\end{aligned}
\tag{17}
$$

The generalized Khrgian and Mazin distribution [12] was first proposed to describe cloud droplets. It is given by

$$
n(r) = ar^\alpha \exp\{-br^\gamma\},
\tag{18}
$$

where the quantities a, b, α, and γ are positive and real constants. These four constants make the distribution general and powerful and allow one to model a wide variety of diverse aerosol phenomena. For a particular choice of α and γ, the constants a and b can be uniquely determined in terms of the total number of particles N per unit volume and the critical or mode radius r_c. For example,

$$
\frac{d}{dr} n(r) = ar^{\alpha-1}(\alpha - \gamma br^\gamma)\exp(-br^\gamma).
\tag{19}
$$

Setting this equal to zero at $r = r_c$, where the concentration is at a maximum, one obtains

$$
b = \alpha/\gamma r_c^\gamma.
\tag{20}
$$

Furthermore, integrating Eq. (18) over the entire range of radii, we get

$$
N = a \int_0^\infty r^\alpha \exp\left[-br^\gamma\right] dr.
\tag{21}
$$

Thus using the notation Γ for the gamma function we have

$$
a = N\gamma b^{(\alpha+1)/\gamma} \Big/ \Gamma\left(\frac{\alpha+1}{\gamma}\right),
\tag{22}
$$

which shows that for a particular choice of α and γ and the use of Eq. (20), the constant "a" is found from the knowledge of N. In particular, with the choice of $\alpha = 6$, $\gamma = 1$, $r_c = 4$ μm, and $N = 100$ cm^{-3}, Deirmendjian [7] obtains the cumulus cloud model

$$
n(r) = 2.373 r^6 e^{-1.5r} cm^{-3} \mu m^{-1},
\tag{23}
$$

and with $\alpha = 1$, $\gamma = 1/2$, $r_c = 0.05$ μm, and $N = 100$ cm^{-3}, he obtains the coastal haze model

$$n(r) = 5.33 \times 10^4 re^{-8.944\sqrt{r}} \ . \tag{24}$$

SAMPLE APPLICATIONS TO HAZE AND DUST

In order to illustrate the varied conditions to which the ASL scattering model may be applied, three representative aerosols were chosen for analysis: (1) an inland continental haze, (2) a coastal haze and (3) dust. The coastal aerosol is represented by the Deirmendjian haze M, which in turn is a particular Khrgian & Mazin with $\alpha = 1$ and $\gamma = 1/2$. The Mie parameters were integrated over the distribution between $r_1 = 0.005$ μm and $r_2 = 4.0$ μm in $\Delta r = 0.01$ μm increments. For illustration purposes only, the haze particles were treated as pure water droplets and the refractive index of pure water was taken from Hale and Querry [13]. The total number density of particles used in these calculations was 100 cm^{-3}. The results are presented in Figures 1 and 2.

Figure 1 is a plot of the Mie absorption, scattering, and extinction cross sections versus wavelength for the spectral region 0.4-14 μm. There are regions of absorption centered around 3 μm and 6 μm, and starting at 10.5 μm and increasing steadily to 14 μm. In the visible region, the greatest loss is due to scattering. However, scattering is also predominant between the narrow absorption regions at 3 and 6 μm. Figure 2 shows the resulting transmittance over a 1-km horizontal path.

The inland continental aerosol is represented by the model C haze of Deirmendjian, which is a modified Junge distribution. The Mie parameters were integrated between $r_1 = 0.03$ μm and $r_2 = 5$ μm in $\Delta r = 0.01$ μm increments. The refractive index of dust was taken from Ivlev and Popova [14]. The total number density of particles used in these calculations was $1.378 \cdot 10^4$ cm^{-3} corresponding to a ground visibility of 5 km [15]. The results are presented in Figures 3 and 4.

Figure 3 shows the Mie absorption, scattering, and extinction cross sections versus wavelength for the spectral region 0.4-14 μm. Regions of absorption exist at 3, 7, 9, and 11.5 μm. Scattering dominates below 6 μm, especially in the visible region.

Figure 1. Plot of the Mie absorption (C_{abs}), scattering (C_{sca}), and extinction (C_{ext}) cross sections vs wavelength for a coastal haze.

Figure 2. Plot of transmittance in a coastal haze over a 1-km horizontal path at sea level vs wavelength; particle number density = 100 cm $^{-1}$.
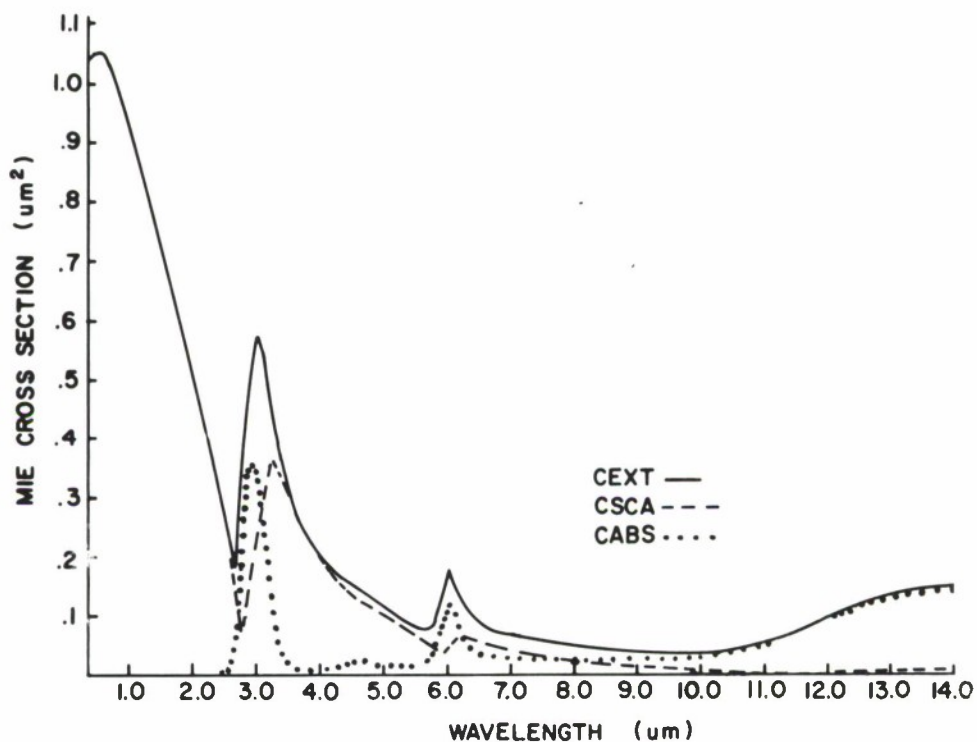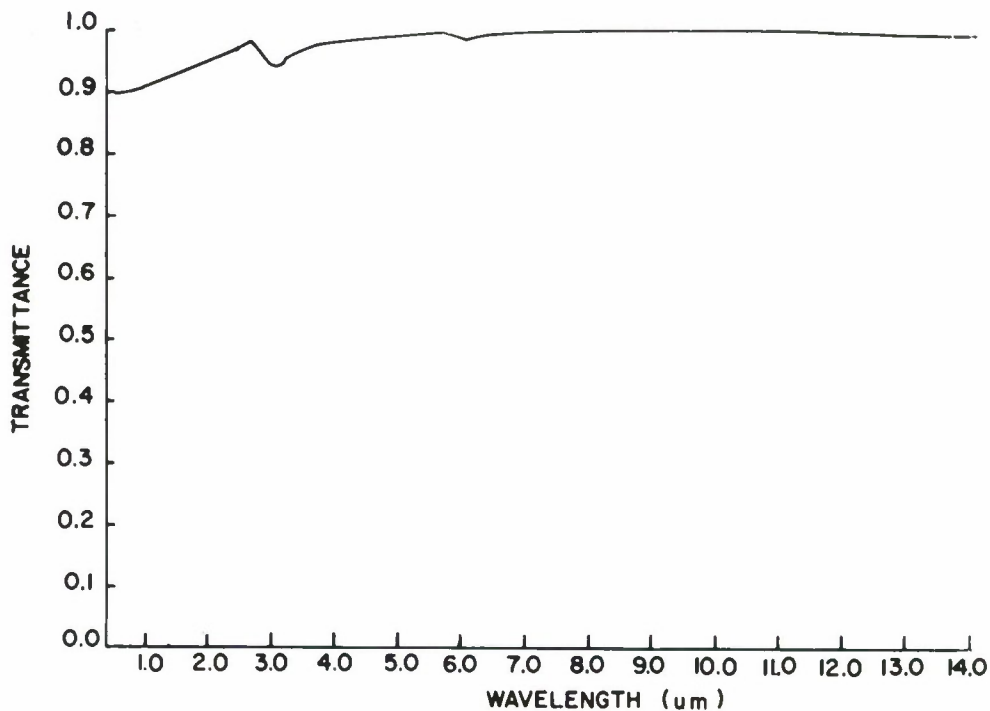
9

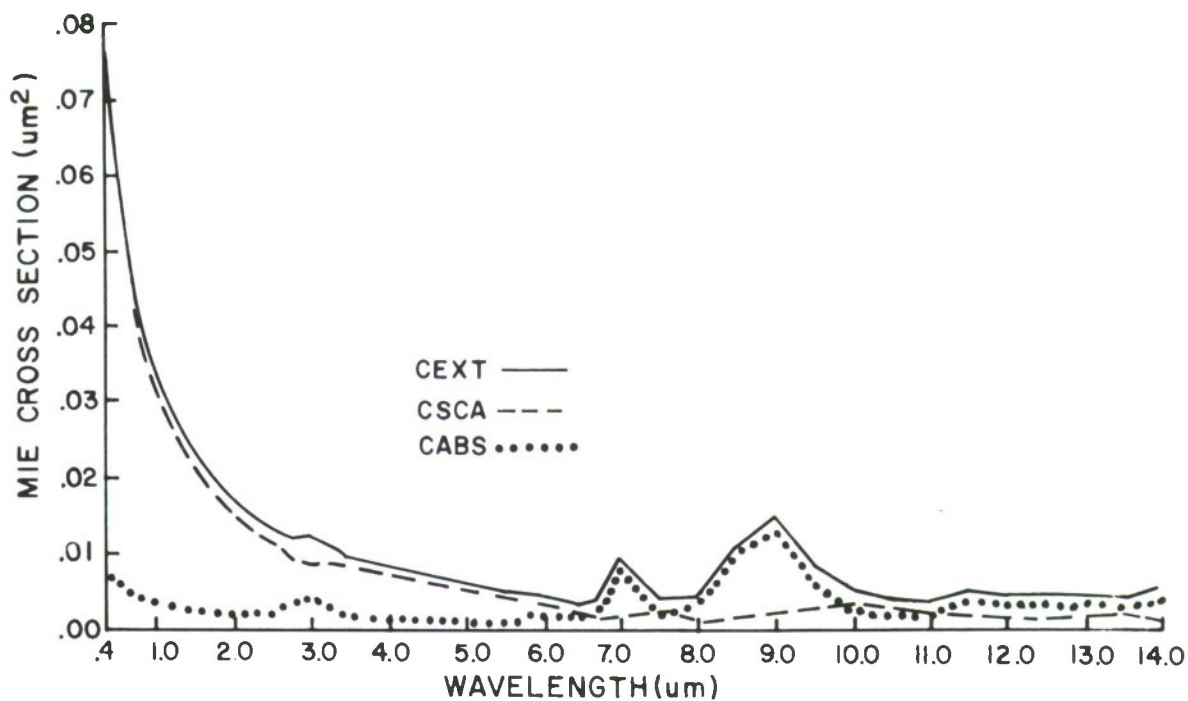Figure 3. Plot of the Mie absorption (C_{abs}), scattering (C_{sca}), and extinction (C_{ext}) cross sections vs wavelength for an inland haze.
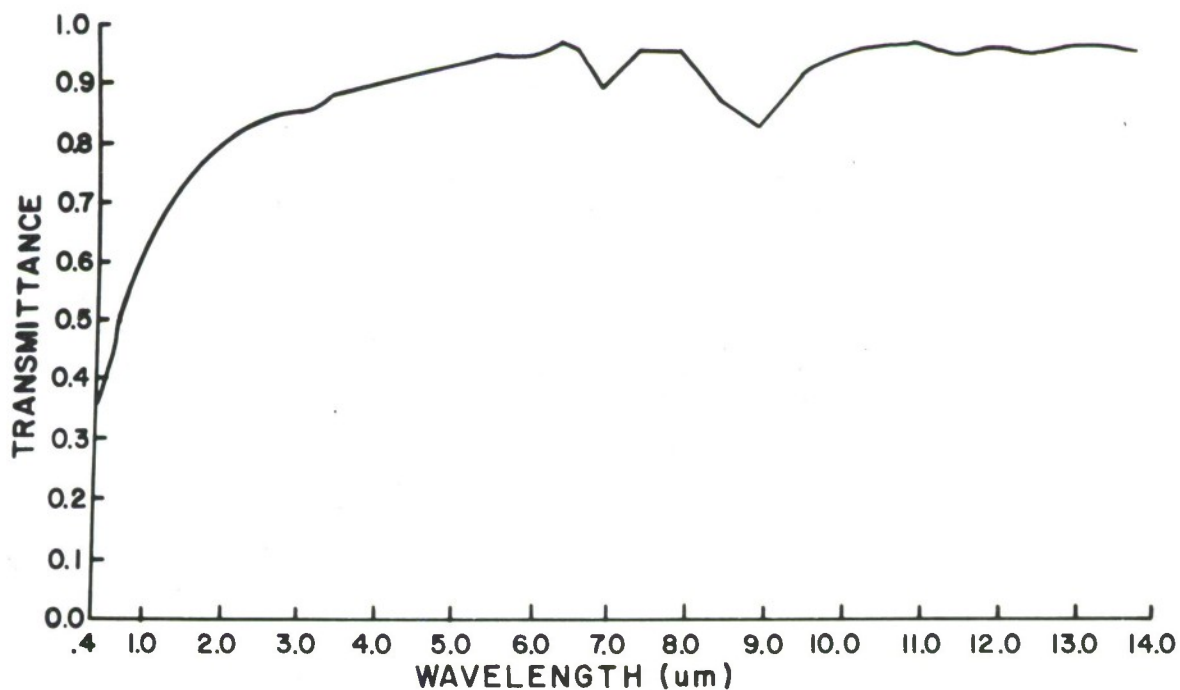

Figure 4. Plot of transmittance in an inland haze over a 1-km horizontal path at sea level vs wavelength; visibility = 5 km.

In Figure 4 we have plotted the resulting transmittance versus wavelength for a 1-km path length. Through the visible region, the transmittance increases essentially linearly from T = 0.33 at 0.4 μm to T = 0.56 at 0.7 μm.

Dust was chosen as representative of a dry, localized aerosol. The distribution used for the giant and large particles is a power law with β=4 and C=30 cm^{-3}, and for the smaller particles a constant with C^1=10^{5}cm^{-3}. However, since the size distributions are internally normalized to unity, number density information must be provided. The number concentration of dust particles was related to visibility by Henley and Hoidale [11] in the following manner:

$$N = \frac{1.1}{V} \cdot 10^5 \text{cm}^{-3} \ , \tag{25}$$

where V is the visibility in km and N the total number density. Values used for the refractive index of dust were obtained from Ivlev and Popova [14] and a visibility of 1 km was used. The results are summarized in Figures 5 and 6.

Figure 5 is a plot of the Mie cross sections versus wavelength for the 0.4-μm to 12-μm spectral region. Note the absorption peaks at 7, 9, and 11.5 μm which influence the total extinction cross section. As expected, scattering is dominant below 2 μm, especially in the visible region. Figure 6 shows the transmittance versus wavelength over the spectral region for a 1-km path length. The transmittance is zero through the visible to 1.5 μm. It then increases steadily to T = 0.23 at 6 μm. Between 6 and 12 μm, absorption bands reduce the values of transmission to T = 0.04 at 7 μm, T = 0.01 at 9 μm, and T = 0.18 at 11.5 μm.

ROLE OF ASL MODEL IN RADIATIVE TRANSFER THEORY

The electromagnetic radiation field in the visible and infrared spectral regions of the Earth's atmosphere depends upon three factors: (1) the natural and/or artificial sources of radiation, (2) the state of the atmosphere, and (3) the surface conditions.

During the day the most important source of natural radiation in the visible and near-infrared part of the spectrum is the sun. In fact, more than 99% of the solar radiation is contained within the spectral band 0.2-4.0 μm. Out to approximately 15 μm the main source of natural

11
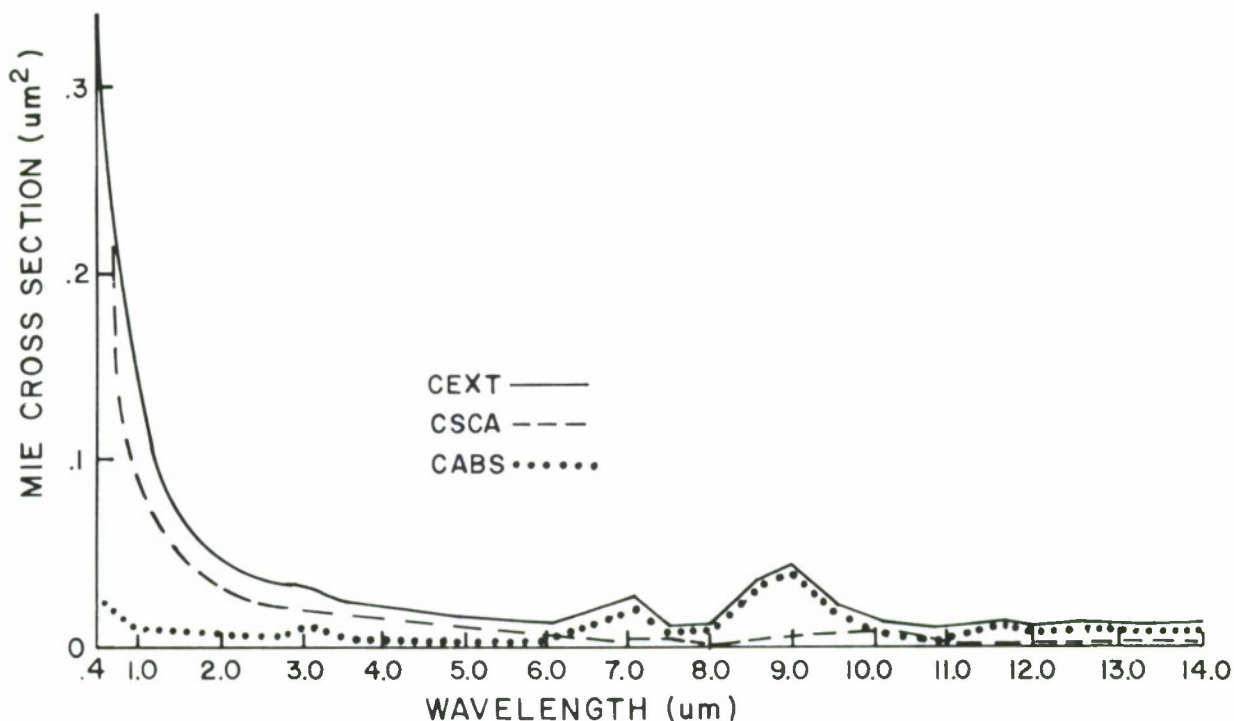
Figure 5. Plot of the Mie absorption (C_{abs}), scattering (C_{sca}), and extinction (C_{ext}) cross sections vs wavelength for a dust haze.
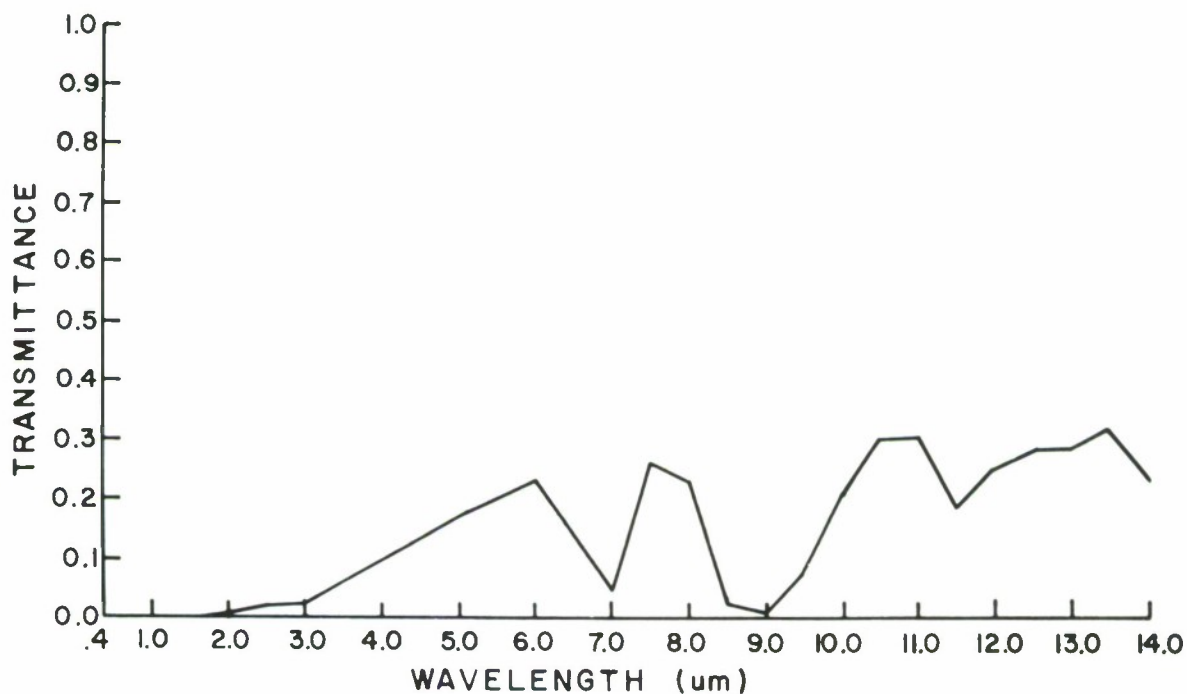

Figure 6. Plot of transmittance vs wavelength in a dust haze for a 1-km horizontal path at sea level; visibility = 1 km.

12

radiation is the Earth's surface. About 30% of the incoming solar radiation is reflected by clouds, dust, and the Earth's surface, whereas 20% is absorbed by the atmosphere. The remaining 50% is absorbed by the Earth. The consequent emission spectrum of the Earth is that of a black body with an effective temperature of 255°K with a peak in the spectrum at 12 μm.

During the night the predominant sources of natural radiation are the moon, stars, airglow in the visible and near-infrared portions of the spectrum, and thermal radiation in the 12-μm region. The intensity of the full moon is about 10^{-6} that of the sun and varies in a known manner with the time of the month. Secondary sources of radiation are those arising from the scattering or absorption of radiation by the atmosphere and the ground. This includes illumination of the surface by light reflected by clouds and the atmosphere. Artificial sources of radiation include lasers, searchlights, flares, and thermal radiation from fires, engines, and other man-made devices. The transfer of all this radiation through the atmosphere is described by radiative transfer models, while the relevant parameters used by these models are described by scatterin models such as the ASL model.

In the last 15 years many different radiation models have been developed for calculating the radiation field existing within the atmosphere.

To illustrate the role that the ASL scattering model plays in radiative transfer theory, described below is a radiative transfer model developed by Turner [16] which is useful for determining spectral radiance and irradiance in real atmospheres.

At the present stage of development, the Turner model will allow one to calculate the spectral sky radiance, spectral path radiance, total spectral radiance, the downwelling diffuse spectral irradiance, the upwelling diffuse spectral irradiance, and the total (direct plus diffuse) downwelling spectral irradiance at any altitude, view angle, solar angle, and for any value of albedo. Also, any wavelength λ except those in the gaseous absorption bands can be used, as can a variety of atmospheric states.

The model is designed for a plane-parallel medium with a very distant point source of radiation incident upon the top of the medium. This point source is usually taken to be the sun, but it could just as well be the moon, a star, or any other source of radiation which approximates a distant point source. The extraterrestrial irradiance values, $E_0(\lambda)$, at the top of the atmosphere were taken from the NASA standard tables of Thekaekara [17].

All calculations are spectral; i.e., the input data and results are given at specific wavelengths, not over bands. In the visible part of the spectrum this is not too important since the spectral variations

13

of the basic optical parameters are small. One could easily simulate the effects of a band - for instance, from 0.55 to 0.60 μm - by taking an average.

Next, one must provide an estimate of the horizontal visual range at the surface. However, it is not necessary to make use of visual range estimates if one has optical depths. The optical depth can be computed with the use of the ASL model. Optical depth is the more fundamental quantity and is preferred over visual range or turbidity. It should be noted that the optical depth is needed for all the wavelengths and altitudes which are desired.

The calculations of the radiometric quantities radiance and irradiance are definitely a function of the reflectance or albedo of the under-lying surface. Hence, one must define the spectral albedo of the sur-face and the spectral reflectance of the target under observation. The spectral albedo for aerosol particles can be calculated with the aid of the ASL model. At the present time only Lambertian surfaces are used with the Turner model, but more general reflectances are being considered.

The altitudes of interest must be specified. Any altitude from 0 to 50 km can be chosen, realizing that the optical depth for all practical purposes is zero at 50 km, the assumed top of the atmosphere.

Finally, one must provide values of the solar zenith angle θ_o, the zenith or nadir view angle θ, and the relative azimuth angle ϕ between the solar plane and the viewing plane.

The major advantages of this model over many others are the following: (1) since the solutions for the basic radiometric parameters are closed-form expressions, the computational time is greatly reduced; and (2) the model can more easily be adapted for a variety of complex environmental situations, such as non-Lambertian targets and vertical and horizontal inhomogeneities.

It should be emphasized that the use of visual range as an index of atmospheric state is just a convenience. If one has available the more fundamental values of optical depth versus altitude versus wavelength for a variety of atmospheric conditions, then these can be used in the model. The single-scattering phase functions (see Appendix), which depend upon wavelength, altitude, and atmospheric condition, are also external inputs to the Turner model. Hence, the important parameters of albedo, optical depth, and phase function are not calculated by the radiative transfer model, but must be introduced to the program by using either a scattering model or experimental values.

14

CONCLUDING REMARKS AND RECOMMENDATIONS

ASL has the capability to model a variety of atmospheric aerosol states
and can calculate or determine the three critical optical parameters –
optical depth, single-scattering albedo, and the single-scattering
phase function. In order to insure compatibility with the input
requirements of the radiative transfer model, the following model
outline is used: As input, the type of aerosol (haze, fog, dust,
etc.) is specified by choosing realistic particle size distributions,
complex refractive indices, and particle number densities. Mie
scattering theory is used to calculate the polydisperse cross sections
C as a function of wavelength and particle radius for complex refractive
index $m(\lambda)$. The combination of total number density with total cross
sections determines the attenuation coefficients: absorption α_{abs},
scattering β_{sca}, and extinction γ_{ext}. These coefficients are then
used to determine transmittance. The single-scattering phase functions
are calculated directly from a knowledge of the spectral complex
refractive index and size distribution. Finally, an integration of
the attenuation coefficients over various altitudes gives the optical
depth as a function of wavelength λ, size distribution n, visibility
V, and altitude z. Also, the single-scattering albedo ω_o can be
calculated from the coefficients. Because of the complexity of the
theoretical modeling, it is recommended that a combined theoretical-
experimental investigation using cloud chambers and laser scattering
experiments be carried out to determine attenuation coefficients and
phase functions for various atmospheric states. Work should continue
to relate the calculated results to a convenient set of available
measurable parameters such as relative humidity, temperature, visual
range, transmissivity, turbidity, contrast transmittance, etc., in
order to define the atmospheric state in an unambiguous way. The
main task in this phase is to study the correlations among the
measurable parameters P_1, P_2, P_3, ... P_L. This parameter set can then
define a unique atmospheric state characterized by $S(n_1, n_2, n_3, ...n_N)$.
As an example, the numbers n_i could be the following:

$n_1 \leftrightarrow$ real refractive index

$n_2 \leftrightarrow$ imaginary refractive index

$n_3 \leftrightarrow$ size distribution parameter #1

$n_4 \leftrightarrow$ size distribution parameter #2

$$n_5 \leftrightarrow \text{size distribution parameter } \#3$$

.
.
.

$$n_i \leftrightarrow \text{particle shape factor } \#1$$

$$n_{i+1} \leftrightarrow \text{particle shape factor } \#2$$

.
.
.

$$n_j \leftrightarrow \text{vertical profile index}$$

$$n_{j+1} \leftrightarrow \text{horizontal inhomogeneity index}$$

.
.

$$n_N$$

Many n_i values are required to define a unique atmospheric condition. For applications to realistic environmental situations, however, it is advisable to combine the n_i values into a smaller set which describes a class of states; e.g.,

$$\underbrace{n_1, \; n_2, \; n_3, \; n_4}_{A_1} \quad \underbrace{n_i \;\; n_{i+1} \cdots n_k}_{A_1} \;\; \underbrace{\cdots n_j}_{\cdots} \;\; \underbrace{n_{j+1} \cdots n_N}_{A_L}$$

$$A_1 \quad\quad\quad A_1 \; . \; . \; . \; A_m \; . \; . \; A_L$$

in which the new set of parameters $(A_1, \ldots A_2, \ldots A_m, \ldots A_L)$ can more easily be identified with the measurable parameter set $(P_1, P_2, \ldots P_L)$. Thus, for a given set of "measurements" or readings in the field, one can specify a subset of possible atmospheric states, and in connection with a suitable radiative transfer model, analysis will allow the radiation field to be determined.

Naturally, the ASL investigation of the radiation field of the atmosphere is not independent of other efforts by other laboratories. We need reflectance models, radiation measurements, etc. Thus, it is recommended that all models being developed under the TSA program be interfaced in this phase of the work, and the resulting combined models validated. These validation studies should include both field and laboratory measurements.

REFERENCES

1. Gomez, R. B., 1972, "Atmospheric Effects for Ground Target Signature Modeling. I: Atmospheric Transmission at 1.06 Micrometers," ECOM-5445, Atmospheric Sciences Laboratory, WSMR, NM.

2. Gillespie, J. B., and C. Petracca, 1974, "Atmospheric Effects for Ground Target Signature Modeling. II: Discussion and Application of a Generalized Molecular Absorption Model," ECOM-5531, Atmospheric Sciences Laboratory, WSMR, NM.

3. Van de Hulst, H. C., 1957, Light Scattering by Small Particles, Wiley, New York.

4. Kerker, M., 1969, The Scattering of Light, Academic Press, New York.

5. Holland, A. C., 1969, "The Scattering of Polarized Light by Polydisperse Systems of Irregular Particles," NASA TN D-5458, NASA, Washington, D.C.

6. Junge, C., 1955, "The Size Distribution and Aging of Natural Aerosols as Determined From Electrical and Optical Data on the Atmosphere," J. of Met., 12, 13-25.

7. Deirmendjian, D., 1959, "Theory of the Solar Aureole. Part II: Applications to Atmospheric Models," Annales De Geophysique, 15, 218-249.

8. Khrgian, A. Kh., and I. P. Mazin, 1952, "The Drop Size Distribution In Clouds," Trudy Tsentral. Aero. Obs. (Moscow), 7, 56-61. (Tech-Trans., 2, (7), 489, 1959; translation: LC No. 59-17161).

9. Khrgian, A. Kh., and I. P. Mazin, 1956, "Analysis of Methods of Characterizing Cloud Droplet Distribution Spectra," Trudy Tsentral. Aero. Obs. (Moscow), 17, 36-46.

10. Green, H. L., and W. R. Lane, 1964, Particulate Clouds: Dusts, Smokes, and Mists, 2nd edition, D. Van Nostrand Company, Inc., Princeton, N.J., 471 pp.

11. Henley, D. C., and G. B. Hoidale, 1973, "Attenuation and Dispersion of Acoustic Energy by Atmospheric Dust," J. Acoust. Soc. Am., 54, 437-445.

12. Mikirov, A. E., "Optical Methods of Determining Distribution Spectra of Particles," Trudy Inst. Priklad. Geofiz. Akad. Nauk SSSR, No. 15, 45-102 (Translation: FSTC-HT-23-1474-73).

13. Hale, G. M., and M. R. Querry, 1973, "Optical Constants of Water in the 200-nm to 200-µm Wavelength Region," Appl. Opt., 12, 555-563.

14. Ivlev, L. S., and S. I. Popova, 1973, "The Complex Refractive Index of the Matter of the Disperse Phase of the Atmospheric Aerosol," Atmos. Ocean. Phys. (Moscow), 9(10), 587-591 (English edition).

15. McClatchey, R. A., et al., 1971,"Optical Properties of the Atmosphere," Environmental Research Papers, No. 354, AFCRL.

16. Turner, R. E., 1973, "Remote Sensing in Hazy Atmosphere," in Remote Sensing of Earth Resources, Vol II, F. Shahrokhi, Ed.

17. Thekaekara, M. P., 1972, "Evaluating the Light from the Sun," March issue of Optical Spectra, 6, 32-35.

18. Mie, G., 1908, "Beitrage Zur Optik Truber Medien, speziell Kolloidaler Metall-Losungen," Ann. Phys., 25, 377-445.

19. Born, M., and E. Wolf, 1959, Principles of Optics, Pergamon Press, New York.

20. Jackson, J. D., 1962, Classical Electrodynamics, Wiley, New York.

21. Stratton, J. A., 1941, Electromagnetic Theory, McGraw-Hill, New York.

22. Ziman, J. M., 1965, Principles of the Theory of Solids, Cambridge University Press, Cambridge, Mass.

23. Shurcliff, W. A., 1962, Polarized Light, Harvard University Press, Cambridge, Mass.

24. Hobson, E. W., 1955, The Theory of Spherical and Ellipsoidal Harmonics, Chelsea, New York.

25. Penndorf, R. B., 1962, "Scattering and Extinction Coefficients for Small Absorbing and Nonabsorbing Aerosols," J. Opt. Soc. Am., 52, 896.

26. Heddle, D.W.O., 1964, "Scattering of Light Near an Absorption Line," J. Opt. Soc. Am., 54, 264.

27. Wills, J. G., 1971, "On the Use of Recursion Relations in the Numerical Evaluation of Spherical Bessel Functions and Coulomb Function," J. Comp. Phys., 8, 162-166.

28. Davis, P., and P. Robinowitz, 1956, "Abscissas and Weights for Gaussian Quadratures of High Order," J. Res. Natl. Bur. Stds., 56, 35-37.

APPENDIX A

MIE THEORY

Mie theory [18] predicts the scattering by and the absorption in an isolated, discrete, homogeneous, isotropic sphere of diameter D with a known complex refractive index $m = n-ik$ relative to the surrounding medium and illuminated by monochromatic radiant energy with wavelength λ in the surrounding medium. The theory is given in detail in standard texts [3, 4, 19-21] and need not be repeated here. Instead, those elements of theory needed for an understanding of the numerical algorithms used in the ASL model are included.

Scatterers attenuate beams of radiant energy by scattering some of the energy into directions other than the incident or forward direction and by absorbing some of the incident energy within the body of the particle. The combined effect of pure scattering by the particle and true absorption within the particle is termed extinction. The amount of extinction, scattering, and absorption by a single particle is given in terms of corresponding equivalent blocking areas or cross sections, C_{ext}, C_{sca}, and C_{abs}, respectively. These cross sections depend only on the refractive index of the particle $m = n-ik$ and the size parameter $\alpha = 2\pi r/\lambda$, where r is the particle radius.

The transmission, T, of a cloud of particles of geometric depth, d, and number density, N, is given by

$$T = e^{-\tau}, \qquad\qquad\qquad\qquad (A-1)$$

with the optical depth, τ, given by

$$\tau = NdC_{ext}, \qquad\qquad\qquad\qquad (A-2)$$

and the cross sections related by

$$C_{ext} = C_{sca} + C_{abs}. \qquad\qquad\qquad\qquad (A-3)$$

When the particle refractive index is real (k = o), the absorption in the particle vanishes; i.e., $C_{abs} = 0$. The balance between loss by scattering and loss by absorption is frequently characterized by the albedo of single scattering ω_0, given by

$$\omega_0 = \frac{C_{sca}}{C_{sca} + C_{abs}} = \frac{C_{sca}}{C_{ext}}. \qquad\qquad\qquad\qquad (A-4)$$

A scatterer with $\omega_0 = 1$ has no absorption and is termed a conservative scatterer. The albedo ω_0 gives the probability that a photon encountering the scatterer will be scattered into some direction including the incident direction.

Although the extinction by a cloud of particles is correctly given by Eqs. (A-1) and (A-2), two implicit assumptions may lead to improper use of the equations. The optical depth τ in Eq. (A-2) does not include losses caused by absorption in the medium surrounding the particles.

This assumption obviously breaks down at wavelengths for which atmospheric gases absorb appreciably. The second assumption is that scattered photons never return to the incident direction. This effect becomes increasingly important as optical depths exceed $\tau = 0.1$.

A final caution should be noted in regard to absorption within the particle. Although absorption within the particle is correctly determined by the wavelength-dependent imaginary part k of the refractive index m, the explicit mechanism which causes the absorption is usually not specified. Texts may be consulted for specific examples [22]. Usually the absorption is joule heating, and it is sometimes necessary to account for the isotropic black body radiation emitted by the scatterer when its temperature rises above that of its surroundings. There may also be circumstances when quantum transitions occur in the scatterer followed by emission at or near the same wavelengths. It is incumbent on the user of the numerical algorithms presented here to properly include these effects since they are not automatically accounted for in these algorithms.

All scattering properties of spheres are computed from n and k, and through the use of the induced electric and magnetic multipole moments of the sphere a_ℓ and b_ℓ, respectively. The moments are given by

$$a_\ell = \frac{\Psi_\ell'(m\alpha)\ \Psi_\ell(\alpha) - m\ \Psi_\ell(m\alpha)\ \Psi_\ell'(\alpha)}{\Psi_\ell'(m\alpha)\ \xi_\ell(\alpha) - m\ \Psi_\ell(m\alpha)\ \xi_\ell'(\alpha)} \tag{A-5}$$

and

$$b_\ell = \frac{m\ \Psi_\ell'(m\alpha)\ \Psi_\ell(\alpha) - \Psi_\ell(m\alpha)\ \Psi_\ell'(\alpha)}{m\ \Psi_\ell'(m\alpha)\ \xi_\ell(\alpha) - \Psi_\ell(m\alpha)\ \xi_\ell'(\alpha)}. \tag{A-6}$$

The prime denotes differentiation with respect to the argument. The $\Psi_\ell(z)$ and $\xi_\ell(z)$ functions are Ricatti-Bessel functions of the first and third kind, respectively, and are related to spherical Bessel functions $j_\ell(z)$ and $n_\ell(z)$ by

$$\Psi_\ell(z) = z\ j_\ell(z) \tag{A-7}$$

and

$$\xi_\ell(z) = z j_\ell(z) - i\ z n_\ell(z), \tag{A-8}$$

where

$$j_\ell(z) = \left(\frac{\pi}{2z}\right)^{1/2} J_{\ell+1/2}(z), \tag{A-9}$$

and

$$n_\ell(z) = \left(\frac{\pi}{2z}\right)^{1/2} N_{\ell+1/2}(z). \tag{A-10}$$

20

The function $J_{\ell+1/2}(z)$ is the half integral order Bessel function; the function $N_{\ell+1/2}(z)$ is the half integral order Neuman function.

The extinction cross section is computed from

$$C_{ext} = \frac{\lambda^2}{2\pi} \sum_{\ell=1}^{\infty} (2\ell+1) \text{ Re } (a_\ell + b_\ell) \tag{A-11}$$

and the scattering cross section from

$$C_{sca} = \frac{\lambda^2}{2\pi} \sum_{\ell=1}^{\infty} (2\ell+1) [|a_\ell|^2 + |b_\ell|^2]. \tag{A-12}$$

The various cross sections are the basic quantities used in scattering problems, but they are not the quantities usually computed directly from Mie algorithms. Instead, it is more convenient to compute dimensionless efficiency factors Q_{ext} and Q_{abs}, which depend on n, k, and α, and which are multiplied by the geometrical sphere cross section to obtain the true cross section $C_i = \pi r^2 Q_i$.

Although the cross sections account for the energy removed from the forward beam, they do not give any information about where the scattered photons go. This information is contained in scattering amplitudes and intensity factors which relate the flux density scattered through an angle θ relative to the incident flux density. There are two amplitudes, $S_1(\theta)$ and $S_2(\theta)$, and intensity factors, $i_1(\theta)$ and $i_2(\theta)$, which correspond to light respectively polarized perpendicular and parallel to the plane of scattering defined by the direction of incidence and the direction of scattering. The ratio of incident to scattered density at radius r from the sphere is given for perpendicular polarization by

$$\frac{I_r}{I_{ro}} = \frac{\lambda^2 i_1 (\theta)}{4\pi^2 r^2} \tag{A-13}$$

and for parallel polarization by

$$\frac{I_\ell}{I_{\ell o}} = \frac{\lambda^2 i_2 (\theta)}{4\pi^2 r^2}. \tag{A-14}$$

21

The intensity factors are related to the scattering amplitudes by

$$i_1(\theta) = |S_1(\theta)|^2 \tag{A-15}$$

and

$$i_2(\theta) = |S_2(\theta)|^2. \tag{A-16}$$

The amplitudes come from the multipole moments through

$$S_1(\theta) = \sum_{\ell=1}^{\infty} \frac{2\ell+1}{\ell(\ell+1)} [a_\ell \pi_\ell(\theta) + b_\ell \tau_\ell(\theta)] \tag{A-17}$$

and

$$S_2(\theta) = \sum_{\ell=1}^{\infty} \frac{2\ell+1}{\ell(\ell+1)} [b_\ell \pi_\ell(\theta) + a_\ell \tau_\ell(\theta)], \tag{A-18}$$

and angular factors $\pi_\ell(\theta)$ and $\tau_\ell(\theta)$ defined in terms of associated Legendre functions:

$$\pi_\ell(\theta) = P_\ell^1(\cos\theta)/\sin\theta; \tag{A-19}$$

$$\tau_\ell(\theta) = \frac{dP_\ell^1(\cos\theta)}{d\theta}. \tag{A-20}$$

The amplitudes have relative phase $\delta = \arg S_1 - \arg S_2$.

Alternative expressions frequently used are

$$\pi_\ell(\theta) = \frac{dP_\ell(\cos\theta)}{d(\cos\theta)} \tag{A-21}$$

and

$$\pi_\ell(\theta) = \cos\theta \cdot \pi_\ell(\theta) - \sin^2\theta \cdot \frac{d\pi_\ell(\theta)}{d(\cos\theta)}, \tag{A-22}$$

where

$$P_\ell(\cos\theta) = \frac{1}{2^\ell \ell!} \frac{d^\ell}{d\cos^\ell\theta}(\cos^2\theta - 1)^\ell. \tag{A-23}$$

22

These functions satisfy the following recurrence relations:

$$\pi_\ell(\theta) = \cos\theta \frac{(2_\ell - 1)}{(\ell-1)} \pi_{\ell-1}(\theta) - \frac{\ell}{\ell-1} \pi_{\ell-2}(\theta) \qquad (A-24)$$

and

$$\tau_\ell(\theta) = \cos\theta [\pi_\ell(\theta) - \pi_{\ell-2}(\theta)] - (2\ell-1)\sin^2\theta \pi_{\ell-1}(\theta) + \tau_{\ell-2}(\theta), \qquad (A-25)$$

with

$$\pi_0(\theta) = 0, \qquad\qquad \tau_0(\theta) = 0,$$

$$\pi_1(\theta) = 1, \qquad\qquad \tau_1(\theta) = \cos\theta,$$

$$\pi_2(\theta) = 3\cos\theta, \qquad\qquad \tau_2(\theta) = 3\cos 2\theta.$$

The scattering cross section measures the ability of a particle to scatter light, and it is to be expected that C_{sca} is obtained from an integral over the scattering intensity factors. Equation (A-12) follows from

$$C_{sca} = \frac{\lambda^2}{4\pi} \int_{-1}^{1} (i_1(\theta) + i_2(\theta)) \, d\cos\theta. \qquad (A-26)$$

Although the intensity factors themselves may be used in scattering calculations, they are primarily suited for computing flux densities, and it is frequently more convenient to measure and compute scattered light in terms of radiances. Radiances do not have the $1/r^2$ dependence, and it is therefore unnecessary to know the distance from the scatterer to the detector if the detector field of view is small and is filled by the scattering cloud. The phase function $p(\theta)$ gives a radiance I scattered into the θ direction in terms of the radiance I_o incident on the particle.

The phase function is dimensionless and is defined here as

$$p(\theta) = \frac{\lambda^2}{2\pi C_{ext}} \left[i_1(\theta) + i_2(\theta) \right]. \qquad (A-27)$$

23

The normalized phase function $p(\theta)d\Omega/4\pi$ gives the probability of a photon being scattered through an angle θ into an element of solid angle $d\Omega = d\phi d\cos\theta$. The integral of the normalized phase function is the single scattering albedo ω_o, which gives the probability that the photon is scattered:

$$\omega_o = \frac{1}{4\pi} \int_0^{2\pi} \int_{-1}^{1} p(\theta)d\phi d\cos\theta = \frac{\lambda^2}{4\pi C_{ext}} \int_{-1}^{1} \left[i_1(\theta)+i_2(\theta) \right] d\cos\theta \qquad (A-28)$$

or

$$\omega_o = C_{sca}/C_{ext}. \qquad (A-29)$$

The phase function contains a sum over the polarization states implicit in the i_1 and i_2 intensity factors, and is thus unsuitable for describing the polarization of the scattered light. Stokes vectors and Mueller matrices [3, 23] are a particularly convenient way to represent polarized light beams and their interaction with scatterers and optical devices. In this context the phase function is replaced by a particular Mueller matrix – namely, the phase matrix.

Stokes vectors and Mueller matrices can be variously defined. Here we use the notation of Van de Hulst [3]. Van de Hulst writes the Stokes elements as time averages of horizontal and vertical electric field components:

$$E_\ell = a_\ell e^{-i\epsilon_1}e^{-ik_o z+i\omega t}; \qquad (A-30)$$

$$E_r = a_r e^{-i\epsilon_2}e^{-ik_o z+i\omega t}; \qquad (A-31)$$

$$I = I_\ell + I_r = a_\ell^2 + a_r^2 ; \qquad (A-32)$$

$$Q = I_\ell - I_r = a_\ell^2 + a_r^2 ; \qquad (A-33)$$

$$U = 2a_\ell a_r \cos\delta; \qquad (A-34)$$

$$V = 2a_\ell a_r \sin\delta; \qquad (A-35)$$

$$\delta = \epsilon_1 - \epsilon_2. \qquad (A-36)$$

24

Here r and ℓ refer to the electric fields perpendicular and parallel with the plane of scattering, k_o is the propagation constant, ω is the angular frequency, (a_ℓ, a_r) are the positive amplitudes of (E_ℓ, E_r), respectively, and $(\varepsilon_1, \varepsilon_2)$ are the corresponding phases of the waves. Furthermore, the electric vector is given by

$$\underset{\sim}{E} = \text{Re}[E_\ell \hat{\ell} + E_r \hat{r}], \qquad (A-37)$$

and the sense is chosen so that $\hat{r} \times \hat{\ell}$ is in the direction of propagation.

As viewed from a detector, these elements in general represent an elliptically polarized beam with its major axis at an angle χ with the horizontal reference axis and with ratio of minor to major axis tangent β. The corresponding elements of the Stokes vector are

$$I = a^2; \qquad (A-38)$$

$$Q = a^2 \cos 2\beta \cos 2\chi; \qquad (A-39)$$

$$U = a^2 \cos 2\beta \sin 2\chi; \qquad (A-40)$$

$$V = a^2 \sin 2\beta. \qquad (A-41)$$

For plane-polarized light, $\beta = 0$ and V vanishes. β is $+\pi/4$ for right circular and $-\pi/4$ for left circular polarized light. The tangent of the phase difference δ (Eq. (A-36)) is

$$\tan \delta = \tan 2\beta / \sin 2\chi. \qquad (A-42)$$

Stokes vectors add linearly, so that a partially polarized beam is represented by the sum of an unpolarized beam $\{I_u, 0, 0, 0\}$ with a completely polarized beam $\{I_p, Q, U, V\}$. This gives an inequality

$$I^2 = (I_u + I_p)^2 \geq Q^2 + U^2 + V^2, \qquad (A-43)$$

which becomes an equality when $I_u = 0$ and the beam is completely polarized. The plane of polarization is given by $U/Q = \tan 2\chi$, and the degree of polarization is $[Q^2 + U^2 + V^2]^{1/2}/I$.

25

Mueller matrices are four-by-four matrices which transform an incident Stokes vector into an outgoing Stokes vector:

$$\{I,\ Q,\ U,\ V\} = M\{I_o,\ Q_o,\ U_o,\ V_o\}. \tag{A-44}$$

When the Stokes vector represents a radiance and M represents a Mie scatterer, M is the phase matrix

$$M = \frac{\lambda^2}{\pi C_{ext}} \cdot \begin{bmatrix} (1/2)(i_2+i_1) & (1/2)(i_2-i_1) & 0 & 0 \\ (1/2)(i_2-i_1) & (1/2)(i_2+i_1) & 0 & 0 \\ 0 & 0 & i_3\cos\delta & -i_3\sin\delta \\ 0 & 0 & i_3\sin\delta & i_3\cos\delta \end{bmatrix} \tag{A-45}$$

in which $i_3 = (i_1 \cdot i_2)^{1/2}$, and δ is the difference in phase between amplitudes $S_1(\theta)$ and $S_2(\theta)$. The corresponding phase matrix for the Stokes vector $\{I_\ell,\ I_r,\ U,\ V\}$ is

$$M' = \frac{\lambda^2}{\pi C_{ext}} \begin{bmatrix} i_2 & 0 & 0 & 0 \\ 0 & i_1 & 0 & 0 \\ 0 & 0 & i_3\cos\delta & -i_3\sin\delta \\ 0 & 0 & i_3\sin\delta & i_3\cos\delta \end{bmatrix} \cdot \tag{A-46}$$

The two phase matrices and all corresponding Mueller matrices are related by similarity transforms

$$M' = T^{-1} MT, \tag{A-47}$$

$$M = TM'T^{-1}, \tag{A-48}$$

with transform matrices

$$T = \begin{bmatrix} 1 & 1 & 0 & 0 \\ 1 & -1 & 0 & 0 \\ 0 & 0 & 1 & 0 \\ 0 & 0 & 0 & 1 \end{bmatrix} \tag{A-49}$$

and

$$T^{-1} = \begin{bmatrix} 1/2 & 1/2 & 0 & 0 \\ 1/2 & -1/2 & 0 & 0 \\ 0 & 0 & 1 & 0 \\ 0 & 0 & 0 & 1 \end{bmatrix}$$

(A-50)

These matrices also transform the Stokes vectors themselves:

$$\{I_\ell,\ I_r,\ U,\ V\} = T^{-1}\{I,\ Q,\ V,\ U\};$$

(A-51)

$$\{I,\ Q,\ U,\ V\} = T\{I_\ell,\ I_v,\ U,\ V\}.$$

(A-52)

The orientation of the horizontal or reference axis implicit in a Stokes vector is quite arbitrary, and it is often necessary to transform to a new reference axis. This may be done by rotating either the Stokes vector or by applying the rotation matrix to the Mueller matrix in a similarity transformation. The rotation matrix

$$L(\phi) = \begin{bmatrix} 1 & 0 & 0 & 0 \\ 0 & \cos2\phi & \sin2\phi & 0 \\ 0 & -\sin2\phi & \cos2\phi & 0 \\ 0 & 0 & 0 & 1 \end{bmatrix}$$

(A-53)

rotates the axes clockwise through the angle ϕ. The inverse transform $L^{-1}(\phi)$ is $L(-\phi)$, so that Mueller matrices transform as

$$M_1 = L(-\phi)M_0\ L(\phi).$$

(A-54)

Although it is unnecessary for single scattering calculations, multiple scattering calculations are usually done in a system of coordinates embedded in an atmosphere rather than attached to each individual scatterer or to a particular source-scatterer-detector combination. Accordingly, it is desirable to find an expression for the phase function and phase matrix in which the dependence on scattering angle θ is replaced by dependence on incoming and outgoing polar angles ν and azimuths ϕ. Thus,

27

if incoming and outgoing directions are denoted by (ν_o, ϕ_o) and (ν, ϕ), respectively, they are related to the scattering angle by

$$\cos(\theta) = \mu\mu_o + (1-\mu^2)^{1/2}(1-\mu_o^2)^{1/2}\cos(\phi-\phi_o), \qquad (A-55)$$

where $\mu=\cos\nu$ and $\mu_o=\cos\nu_o$. The corresponding transformation for the phase function is obtained by expanding it in a Legendre series:

$$p(\theta) = \sum_{\ell=0}^{N} \omega_\ell P_\ell(\cos\theta), \qquad (A-56)$$

with coefficients ω_ℓ given by

$$\omega_\ell = \frac{2\ell+1}{2} \int_{-1}^{1} p(\theta) \, P_\ell(\cos\theta) d\cos\theta \qquad (A-57)$$

and Legendre polynomials $P_\ell(\cos\theta)$. When $p(\theta)$ is normalized, ω_o is again the single scattering albedo. The transformation of $p(\theta)$ into $p(\mu, \phi, \mu_o, \phi_o)$ follows from the addition theorem for Legendre polynomials [24]:

$$p(\mu,\phi,\mu_o,\phi_o) = \sum_{\ell=o}^{N} \omega_\ell \left[P_\ell(\mu)P_\ell(\mu_o) \right.$$

$$\left. + 2 \sum_{m=1}^{\ell} \frac{(\ell-m)!}{(\ell+m)!} P_\ell^m(\mu)P_\ell^m(\mu_o)\cos m(\phi-\phi_o) \right]. \qquad (A-58)$$

Inversion of the order of summation gives

$$p(\mu,\phi,\mu_o,\phi_o) = \sum_{m=o}^{N} (2-\delta_o^m) [\sum_{\ell=m}^{N} \omega_\ell \frac{(\ell-m)!}{(\ell+m)!} P_\ell^m(\mu) \, P_\ell^m(\mu_o)]\cos m(\phi-\phi_o), \qquad (A-59)$$

where δ_o^m is the Kronecker delta. The corresponding expressions for the phase matrix M are considerably more difficult, and their discussion will be included in a report which discusses multiple scattering. The phase function transformation (Eqs. (A-56) and (A-57)) is included here since it is incorporated in the algorithm used in the ASL scattering code.

The sequence of multipole moments $a_1,\ldots,b_1,\ldots$ is notoriously slow to converge since at least α terms are needed. For economy reasons,

28

approximations are frequently used to avoid the Mie formalism. Van de Hulst [3] and Kerker [4] give a number of approximations commonly used and discuss their ranges of validity and their error penalties. Of those approximations, Rayleigh scattering, valid for particles small with respect to incident wavelength, is probably the one most commonly used. Two forms of this approximation are included here: one which describes scattering by small, discrete spheres, and one which describes scattering by gaseous molecules.

Penndorf [25] has derived approximate equations for the efficiency factors Q_{ext}, Q_{sca}, and Q_{abs} by expanding the Mie multipole moments a_1, b_1, a_2, b_2, and a_3 into polynomials in α for complex refractive index $m = n-ik = n(1-i\kappa)$. The result for the extinction efficiency factor is

$$Q_{ext} = \frac{24n^2\kappa}{z_1}\,\alpha + \left\{ \frac{4n^2\kappa}{15} + \frac{20n^2\kappa}{3z_2} + 4.8n^2\kappa\left[\frac{7(n^2+n^2\kappa^2)^2+4(n^2-n^2\kappa^2-5)}{z_1^2}\right]\right\}\alpha^3$$

$$+ \frac{8}{3}\left\{\frac{[(n^2+n^2\kappa^2)^2+(n^2-n^2\kappa^2-2)]^2-36n^4\kappa^2}{z_1^2}\right\}\alpha^4, \tag{A-60}$$

with

$$z_1 = (n^2+n^2\kappa^2)^2 + 4(n^2-n^2\kappa^2)+4 \tag{A-61}$$

and

$$z_2 = 4(n^2+n^2\kappa^2)^2 + 12(n^2-n^2\kappa^2)+9. \tag{A-62}$$

The scattering efficiency factor is

$$Q_{sca} = (8/3z_1^2)\{[(n^2+n^2\kappa^2)^2+n^2-n^2\kappa^2-2]^2+36n^4\kappa^2\}\alpha^4$$

$$\cdot\{1+(6/5z_1)\,[(n^2+n^2\kappa^2)^2-4]\,\alpha^2-(24n^2\kappa\alpha^3/3z_1)\}, \tag{A-63}$$

and the absorption efficiency factor is

$$Q_{abs} = (24n^2\kappa\alpha/z_1) + \left\{ \frac{4n^2\kappa}{15} + \frac{20n^2\kappa}{3z_2} + 4.8n^2\kappa\left[\frac{7(n^2+n^2\kappa^2)^2+4(n^2-n^2\kappa^2-5)}{z_1^2}\right]\right\}\alpha^3$$

$$-192(n^2\kappa/z_1)^2\alpha^4 \tag{A-64}$$

29

or

$$Q_{abs} \simeq Im \left[-4\alpha \left(\frac{m^2-1}{m^2+2}\right) \right] .$$ (A-65)

For nonabsorbing spheres ($\kappa=0$), the scattering efficiency factor (for small size parameters) reduces to

$$Q_{sca} = Q_{ext} = \frac{8\alpha^4}{3} \left(\frac{n^2-1}{n^2+2}\right)^2 \left\{ 1 + \frac{6}{5} \alpha^2 \left(\frac{n^2-2}{n^2+2}\right) \right.$$

$$+ \alpha^4 \left[\frac{3}{175} \left(\frac{n^6+41n^4-284n^2+284}{(n^2+2)^2}\right) \right.$$

$$\left. \left. + \frac{1}{900} \left(\frac{n^2+2}{2n^2+3}\right)^2 (15 + (2n^2+3)^2) \right] \right\} .$$ (A-66)

In quoting these approximations, Kerker [4] suggests that for $\kappa = 0$ these equations may be used for values of $\alpha \leq 1.4$ and $m \leq 2$. The error incurred is less that 2% for $m \leq 1.5$, but may reach 15% at $m = 2$. For absorbing spheres the approximations are useful for $\alpha \leq 0.8$ in the range $1.25 \leq n \leq 1.75$ and $n\kappa \leq 1$.

Van de Hulst [3] has given equations for cross sections for clouds of N anisotropic molecules with random orientations. For a gas with refractive index $m = n-ik$, the absorption cross section is

$$C_{ext} = \frac{4\pi k}{\lambda N} ,$$ (A-67)

which gives the usual absorption coefficient for gases:

$$NC_{ext} = 4\pi k/\lambda .$$ (A-68)

The corresponding scattering cross section is given by

$$C_{sca} = \frac{8\pi^3 f}{3\lambda^4 N^2} [(n^2-1)^2+4k^2] ,$$ (A-69)

30

in which f is the Cabannes factor (f = 1.054 for air). For k=0, Eq. (A-69) reduces to the value given by Van de Hulst for nonabsorbing gases. The derivation for absorbing gas cross sections, when done in two apparently equivalent ways, leads to the $4k^2$ term being either positive or negative. The positive choice here is consistent with that of Heddle [26].

<div align="center">PGAUSS PROGRAM</div>

The theory given in the previous portion of the Appendix has been implemented in numerical form as a control routine, PGAUSS, and several subroutines, MIEGSS, GAUSS, VERIFY, and GUSSET. The PGAUSS routine receives wavelength-dependent refractive index data and definitions of particle size distributions from the user, and employs the subroutines to return scattering and extinction cross sections, phase functions, and phase matrix elements for the poly-dispersion. PGAUSS is an extremely versatile routine since it can be used to generate Mie functions for arbitrary mono- and polydispersions, or a variety of standard types of polydispersions for comparatively wide ranges in particle size parameter and refractive index.

The PGAUSS routine consists of three nested control loops. The outer loop indexes GAUSS quadrature orders, the intermediate loop indexes wave-lengths, and the inner loop integrates Mie functions over the size distributions for each wavelength. No integration over wavelength is provided at present, although it would be simple to include it as an option.

The internal size distributions offered as options include entries into an arbitrary, a log-normal, the Deirmendjian [7] haze C, the Junge [6], and the Khrgian and Mazin [8, 9] modified gamma distributions. The distributions each call for their particular input data, and because the distributions n(r) are normalized internally,

$$\int_{r_1}^{r_2} n(r)dr = 1, \tag{A-70}$$

the number density information must be input into the model. The resulting Mie functions are thus equivalent to single (but averaged) particle data.

The Mie functions are computed by the subroutine MIEGSS, which returns extinction and scattering efficiency factors Q_{ext} and Q_{sca}, intensity factors i_1 and i_2, and the relative phase δ of i_1 and i_2 for each complex refractive index m and size parameter α. The Ricatti-Bessel functions and their derivatives in Eqs. (A-5) and (A-6) are presently

<div align="center">31</div>

computed by forward recursion of the χ's and backward recursion of the Ψ's. Start forward recurring using the following: [Note: $\xi_n(z) = \Psi_n(z) + i\chi_n(z)$]

$$\chi_o(z) = \cos z, \tag{A-71}$$

$$\chi_1(z) = \cos z/z + \sin z, \tag{A-72}$$

and the recursion formula

$$f_n(z) = (2n-1)\ f_{n-1}(z)/z - f_{n-2}(z) \tag{A-73}$$

and

$$f_n'(z) = f_{n-1}(z) - (n+1)\ f_n(z)/z. \tag{A-74}$$

If L orders are needed, then the backward recursion is used until L orders of χ's are generated. The recursion is continued, but now the sum

$$S = \sum_{i=n}^{\infty} \frac{1}{\chi_i(z)\chi_{i+1}(z)} \tag{A-75}$$

is formed. This is rapidly converging as soon as n is greater than z.

The sum is converged when successive terms are less than some tolerance; e.g., $L = 10^{-5}$; then from

$$\frac{\Psi_n(z)}{\chi_n(z)} = S_n, \tag{A-76}$$

we may recur backwards using the relations

$$\Psi_L(z) = \chi_L(z) \cdot S_L, \tag{A-77}$$

$$\Psi_{L-1}(z) = \chi_{L-1}(z) \cdot S_L + \frac{1}{\chi_L(z)}\ , \tag{A-78}$$

and the backward recursion

$$\Psi_{n-1}(z) = (2n+1) \ \Psi_n(z)/z - \Psi_{n+1}(z) \qquad \text{(A-79)}$$

to generate the Ψ's. Finally, a scaling factor F is calculated for
$\Psi_o(z)$:

$$F = \Psi_o(z)/\sin z$$

and then all the Ψ's are scaled appropriately. This algorithm is from
Wills [27] and appears to be accurate and stable over the index ranges
of $n\alpha$ used in this report.

The Mie series is terminated either when two successive terms have $|a_n|$
+ $|b_n| < 10^{-5}$, or when the number of terms exceeds $6 + F\alpha$. F is 1.2 for
$\alpha \leq 51$ and is $1. + 2.26\alpha^{-.613}$ for $\alpha > 51$. These cutoff criteria terminate
the series satisfactorily before serious instabilities occur. The 10^{-5}
tolerance should be adjusted to be compatible with the computer
single-word precision. This value is reasonable for 32-bit machines, but
10^{-6} is more appropriate for 36-bit machines and 10^{-11} should suffice for
60-bit machines.

The angular functions $\pi_n(\theta)$ and $\tau_n(\theta)$ are computed by forward recursion
from

$$\pi_n(\theta) = [(2n-1) \ \cos\theta\pi_{n-1}(\theta) - n\pi_{n-2}(\theta)]/(n-1), \qquad \text{(A-80)}$$

$$\rho_n(\theta) = (2n-1) \ \pi_{n-1}(\theta) + \rho_{n-2}(\theta), \qquad \text{(A-81)}$$

$$\tau_n(\theta) = \pi_n(\theta) \ \cos \ \theta - \sin^2\theta\rho_n(\theta), \qquad \text{(A-82)}$$

and the starting values $\pi_o = 0$, $\rho_o = 0$, $\pi_1 = 1$, and $\rho_1 = 0$.

The Legendre expansions of the integrated phase functions and the phase
matrix elements are provided by subroutine GAUSS. The integral in Eq.
(A-57) is replaced by a Gauss-Legendre sum, so that the expansion
coefficients are given by

$$\omega_\ell = \frac{2\ell+1}{2} \int_{-1}^{1} f(\cos\theta)P_\ell(\cos \ \theta) \ d \cos \ \theta$$

$$= \frac{2\ell+1}{2} \sum_{i=1}^{L} f(\cos\theta_i)P_\ell(\cos\theta_i)d\cos\theta_i w_i. \qquad \text{(A-83)}$$

The replacement is exact (to machine accuracy) when the product in the
integrand is a polynomial in $\cos \ \theta_i$ of degree $2L - 1$ or less. The

order of quadrature L is an input to PGAUSS and should be set at two to
three times the largest size parameter expected in the Mie calculation.

33

The abscissa $\cos \theta_i$ and weights w_i are computed by subroutine GUSSET. The Mie angle-dependent factors are computed at angles corresponding to the $\cos \theta_i$.

In addition to computing the ω_ℓ coefficients, GAUSS reconstructs $p(\cos \theta_i)$ as $p_c(\cos \theta_i)$, and computes an rms distance of $p(\cos \theta_i)$ from $p_c(\cos \theta_i) [\sum_{i=1}^{N} (p(\cos \theta_i) - p_c(\cos \theta_i))^2]^{1/2}$ as each successive term is added to the series (Eq. (A-56)). The distance function is particularly useful in determining the number of terms to be retained in Eq. (A-56) for adequate precision in the expansion. Subroutine VERIFY produces a reconstruction $p_c(\cos \theta_i)$ using the number of terms which minimize the distance function.

The quadrature weights and abscissas are computed by GUSSET in double precision using the Davis and Rabinowitz algorithm [28]. The abscissas $x_{kn} = \cos \theta_{kn}$ are the $k = 1,\ldots, n$ zeros of $P_n(x_{kn}) = 0$, while the weights are given by

$$a_{kn} = 2(1 - x_{kn}^2)^2/[nP_{n-1}(x_{kn})]^2. \tag{A-84}$$

Initial estimates of the zeros are obtained from the j_k successive zeros of the Bessel function $J_o(j_k) = 0$ via

$$x_{kn} = \cos[j_k/((n+1/2)^2 + (1 - (2/\pi)^2)/4)^{1/2}. \tag{A-85}$$

Final values of the x_{kn} are found by Newton-Raphson iteration.

ATMOSPHERIC SCIENCES RESEARCH PAPERS

1. White, Kenneth O., James B. Gillespie, Robert Armstrong, and Larry E. Traylor, "State-of-the-Art Survey of Meteorological Instrumentation Required to Determine Atmospheric Effects on Airborne Laser Tests," ECOM-5469, January 1973.

2. Duncan, Louis D., and Barbara J. Richart, "Mesoscale Variation of Spectral Radiance Near 15 Micrometers," ECOM-5470, January 1973.

3. Schleusener, Stuart A., and Kenneth O. White, "Solid-State Laser Multiwavelength Identification and Display System," ECOM-5473, January 1973.

4. Nordquist, Walter S., Jr., "Numerical Approximations of Selected Meteorological Parameters Related to Cloud Physics," ECOM-5475, March 1973.

5. Maynard, Harry, "An Evaluation of Ten Fast Fourier Transform (FFT) Programs," ECOM-5476, March 1973.

6. Gerber, Hermann E., "Freezing Water with Sized AgI Particles. I: A Survey," ECOM-5477, March 1973.

7. Gerber, Hermann E., "Freezing Water with Sized AgI Particles. II: Theoretical Considerations," ECOM-5478, March 1973.

8. D'Arcy, Edward M., "Accuracy Study of the T-9 Radar," ECOM-5480, March 1973.

9. Miller, Walter B., "An Investigation of Errors Introduced into Meteorological Calculations Through Use of the Hypsometric Equation," ECOM-5481, April 1973.

10. Miller, Walter B., "On Indirect Pressure Estimation from Measurements of Height and Temperature," ECOM-5482, April 1973.

11. Rinehart, G. S., and R. P. Lee, "Apparent 7-Day Period in Visibility Data at White Sands Missile Range, New Mexico," ECOM-5484, April 1973.

12. Swingle, Donald M., and Raymond Bellucci, "Improved Sound Ranging Location of Enemy Artillery," ECOM-5486, April 1973.

13. Lindberg, James D., and David G. Snyder, "Determination of the Optical Absorption Coefficient of Powdered Materials Whose Particle Size Distribution and Refractive Indices Are Not Known," ECOM-5487, April 1973.

14. Rubio, Roberto, "Winter Anomalous Radio Wave Absorption Days at 32°N Latitude and Prevalent Solar Radiation," ECOM-5488, May 1973.

15. Nordquist, W. S., "Data from a Fog Dispersal Experiment Using Helicopter Downwash," ECOM-5456, May 1973.

16. Shinn, Joseph H., "Optimum Wind Soundings and Army Fallout Prediction Accuracies," ECOM-5489, May 1973.

17. Miller, Walter B., and Donald R. Veazey, "An Integrated Error Description of Active and Passive Balloon Tracking Systems," ECOM-5500, June 1973.

18. Doll, Barry, "The Potential Use of Polarized Reflected Light in the Remote Sensing of Soil Moisture," ECOM-5501, July 1973.

19. Duncan, Louis D., "A Geometric Investigation of the Effect of Viewing Angle on the Ground Resolution of Satellite-Borne Sensors," ECOM-5502, July 1973.

20. Miller, Walter B., and Donald R. Veazey, "Vertical Efficiency of Active and Passive Balloon Tracking Systems from a Standpoint of Integrated Error," ECOM-5503, July 1973

21. Richter, Thomas J., "Design Considerations for the Calculator, Altitude ML-646(XE-1)/UM," ECOM-5504, August 1973.

22. Randhawa, J. S., "Measurement of Total Ozone at WSMR, NM," ECOM-5505, August 1973.

23. Mason, James B., "Lidar Measurement of Temperature: A New Approach," ECOM-5506, August 1973.

24. Randhawa, J. S., "An Investigation of Solar Eclipse Effect on the Subpolar Stratosphere," ECOM-5507, September 1973.

25. Wade, Gerald T., Teddy L. Barber, and Robert Armstrong, "A Proposed Versatile Photon Counter System for Laser Radar," ECOM-5508, September 1973.

26. Lentz, W. J., "A New Method of Computing Spherical Bessel Functions of Complex Argument with Tables," ECOM-5509, September 1973.

27. White, Kenneth O., Gerald T. Wade, and Stuart A. Schleusener, "The Application of Minicomputers in Laser Atmospheric Experiments," ECOM-5510, September 1973.

28. Collett, E., R. Alferness, and T. Forbes, "Log-Intensity Correlations of a Laser Beam in a Turbulent Medium," ECOM-5511, September 1973.

29. Robbiani, Raymond L., "Design Concept of a Forward Area Rawinsonde Set (FARS)," ECOM-5512, October 1973.

30. Stone, William J., "The Hydrometeorologic Ground Truth Facility at White Sands Missile Range, New Mexico," ECOM-5513, October 1973.

31. Lacy, Claud H., "Objective Analysis Using Modeled Space-Time Covariances: An Evaluation," ECOM-5514, October 1973.

32. Stipanuk, G. S., "Algorithms for Generating a SKEW-T, log p DIAGRAM and Computing Selected Meteorological Quantities," ECOM-5515, October 1973.

33. Sharenow, Moses, "Test and Evaluation of Natural Rubber Spherical Balloons," ECOM-5516, October 1973.

34. White, Kenneth O., and Gerald T. Wade, "Remote Sensing of Atmospheric Methane Using an Erbium/YAG Laser: A Feasibility Study," ECOM-5517, October 1973.

35. Tchen, Chan Mou, and Edward Collett, "The Spectrum of Laser-Induced Turbulence," ECOM-5518, February 1974.

36. Collett, Edward, and Chan Mou Tchen, "Turbulent Heating of an Atmosphere by a Laser Beam," ECOM-5519, February 1974.

37. Gerber, Hermann E., "Freezing Water with Sized AgI Particles. III: Experimental Procedure, Results, and Conclusions," ECOM-5520, March 1974.

38. Lindberg, James D., "A Simple Method for Measuring Absolute Diffuse Reflectance with a Laboratory Spectrophotometer," ECOM-5521, November 1973.

39. Lindberg, James D., and Michael S. Smith, "Visible and Near Infrared Absorption Coefficients of Kaolinite and Related Clays," ECOM-5522, November 1973.

40. Weathers, L. R., and R. B. Loveland, "Magnetic Field Survey at White Sands Missile Range, New Mexico," ECOM-5523, November 1973.

41. Matonis, Casimir J., "The Potential Use of Tactical Microwave Radio (TMR) for Transmission of Weather Radar Data," ECOM-5524, December 1973.

42. Lindberg, James D., and Larry S. Laude, "A Measurement of the Absorption Coefficient of Atmospheric Dust," ECOM-5525, December 1973.

43. Low, Richard D. H., "Microphysical and Meteorological Measurements of Fog Supersaturation," ECOM-5526, December 1973.

44. Nordquist, Walter S., "Fog Clearing Using Helicopter Downdrafts: A Numerical Model," ECOM-5527, December 1973.

45. Lentz, W. J., and G. B. Hoidale, "Estimates of the Extinction of Electromagnetic Energy in the 8 to 12 μm Range by Natural Atmospheric Particulate Matter," ECOM-5528, January 1974.

46. Duncan, Louis D., and Marvin Kays, "Determining Nuclear Fallout Winds from Satellite-Observed Spectral Radiances," ECOM-5529, January 1974.

47. Henley, David C., "An Analysis of Random Fluctuations of Atmospheric Dust Concentrations," ECOM-5530, January 1974.

48. Gillespie, James B., and Carmine Petracca, "Atmospheric Effects for Ground Target Signature Modeling. II. Discussion and Application of a Generalized Molecular Absorption Model," ECOM-5531, January 1974.

49. Anthes, Richard A., and Thomas T. Warner, "Prediction of Mesoscale Flows Over Complex Terrain," ECOM-5532, March 1974.

50. Low, Richard D. H., "Microphysical Evolution of Fog," ECOM-5533, March 1974.

51. Duncan, Louis D., "An Iterative Inversion of the Radiative Transfer Equation for Temperature Profiles," ECOM-5534, March 1974.

52. Blanco, A. J., E. M. D'Arcy, and J. B. Gillespie, "Degradation of a Helium-Neon Laser Beam by Atmospheric Dust During a Sand Storm," ECOM-5535, March 1974.

53. Barr, William C., "An Analysis of Loran Wind-Measuring Accuracies for Application to Field Army Use," ECOM-5536, April 1974.

54. Westwater, E. R., J. B. Snider, A. V. Carlson, and J. R. Yoder, "Experimental Determination of Temperature Profiles by Ground-Based Radiometry," ECOM-5537, April 1974.

55. White, Kenneth O., W. R. Watkins, and S. A. Schleusener, "Measurement of Ho^{3+} :YLF 2.06 μm Laser Spectral Output Variations and CO_2 Absorption Coincidence," ECOM-5538, April 1974.

56. Gillespie, James B., James D. Lindberg, and Michael S. Smith, "Visible and Near-Infrared Absorption Coefficients of Montmorillonite and Related Clays," ECOM-5539, May 1974.

57. Cantor, Israel, "Aerosol Angular Scattering Functions for Model Atmospheres," ECOM-5540, May 1974.

58. Pena, Ricardo, and H. N. Schwartz, "A High Resolution Temperature Sonde for the Lower Atmosphere," ECOM-5541, May 1974.

59. Diderich, Robert A., Kenneth M. Barnett, and Ronald M. Cionco, "Evaluation of Several Wire Mesh Screens for the Protection and Ventilation of Meteorological Sensors," ECOM-5542, May 1974.

60. Miller, Walter B., and Donald R. Veazey, "On Increasing Vertical Efficiency of a Passive Balloon Tracking Device by Optimal Choice of Release Point," ECOM-5543, June 1974.

61. Randhawa, J. S., "Partial Solar Eclipse Effects on Temperature and Wind in an Equatorial Atmosphere," ECOM-5544, June 1974.

62. Duncan, Louis D., "Approximations in Inverting the Radiative Transfer Equation," ECOM-5545, July 1974.

63. Pries, Thomas H., and Erick T. Young, "Evaluation of a Laser Crosswind System," ECOM-5546, July 1974.

64. Shinn, Joseph H., and Harry W. Maynard, "On the Sensitivity of Selected Typical Tactical Army Operations to Weather Effects," ECOM-5547, October 1974.

65. Miller, Walter, and Bernard Engebos, "On Determining Cost-Effectiveness of an Army Automatic Meteorological System," ECOM-5548, November 1974.

66. Conover, Walter, "Operational Techniques for Radar Set AN/TPS-41," ECOM-5549, November 1974.

67. Barber, T. L., and J. B. Mason, "A Transit-Time Lidar Wind Measurement: A Feasibility Study," ECOM-5550, December 1974.

68. Olsen, R. O., and B. W. Kennedy, "The Utilization of Starute Decelerators for Improved Upper Atmosphere Measurements," ECOM-5551, December 1974.

69. Bruce, Rufus E., and Louis D. Duncan, "The Effect of Atmospheric CO_2 Variations on Satellite-Sounded Temperatures," ECOM-5552, December 1974.

70. Thomas, J. E., M. D. Kays, J. D. Horn, and R. L. Moore, "Visual Observation of Propagating Gravity Waves on ATS III Satellite Film Loops," ECOM-5553, January 1975.

71. Ballard, Harold N., and Frank P. Hudson, "Stratospheric Composition Balloon-Borne Experiment - 18 September 1972," ECOM-5554, January 1975.

72. D'Arcy, Edward M., "Some Behavior Characteristics of the Rawinsonde and AN/FPS-16 Radar When Used As Balloon Tracking Devices," ECOM-5555, January 1975.

73. Alexander, George D., "Determining Geostrophic Winds Using A Satellite-Borne Infrared Radiometer," ECOM-5556, February 1975.

74. Miers, B. T., and H. S. Oey, "An Evaluation of the Hydrometeorological Ground Truth Facility at White Sands Missile Range, New Mexico," ECOM-5557, February 1975.

75. Gomez, R. B., Carmine Petracca, Charles Querfeld, and Glenn B. Hoidale, "Atmospheric Effects for Target Signature Modeling. III: Discussion and Application of the ASL Scattering Model," ECOM-5558, March 1975.

DISTRIBUTION LIST

Defense Documentation Center
ATTN: DDC-TCA
Cameron Station (BLDG 5)
Alexandria, Virginia 22314

Commander
US Army Missile Command
ATTN: AMSMI-RE (Mr. Pittman)
Redstone Arsenal, Alabama 35809

Commander
US Army Missile Command
ATTN: AMSMI-RR
Redstone Arsenal, Alabama 35809

Commander
US Army Missile Command
ATTN: AMSMI-RRA, Bldg 7770
Redstone Arsenal, Alabama 35809

Redstone Scientific Info Center
ATTN: Chief, Documents
US Army Missile Command
Redstone Arsenal, Alabama 35809

Chief, Aerospace Enviro Div
Code S&E-AERO-Y
NASA (Mr. Vaughan)
Marshall Space Flight Center,
Alabama 35802

NASA Aero-Astrodynamics Laboratory
ATTN: S&E-AERO-YS
Marshall Space Flight Center,
Alabama 35812

Commander
USAICS
ATTN: ATSI-CTD-MS (Met Branch)
Fort Huachuca, Arizona 85613

Commander
Headquarters, Fort Huachuca
ATTN: Tech Ref Div
Fort Huachuca, Arizona 85613

Dr. Robert Durrenberger
Director, The Laboratory of Climatology
Arizona State University
Tempe, Arizona 85281

Commander
ASL Yuma Met Team
ATTN: Captain Jones
Yuma Proving Ground, Arizona 85364

Commander
Yuma Proving Ground
ATTN: STEYP-AD, Tech. Library
Yuma, Arizona 85364

Fugro National, Inc.
718 East 3rd Street
ATTN: Mr. Jerry Allen
Long Beach, California 90801

Sylvania Elec Sys. Western Div
ATTN: Technical Reports Library
P. O. Box 205
Mountain View, California 94040

Geophysics Officer
Code 3250
Pacific Missile Range
Point Mugu, California 93042

Commander
Naval Electronics Laboratory Center
ATTN: Library
San Diego, California 92152

Director
Atmospheric Physics & Chem Lab
Room 31, NOAA
Department of Commerce
Boulder, Colorado 80302

Library-R-51-Tech Reports
Environmental Research Labs
NOAA
Boulder, Colorado 80302

National Center for Atmos Res
NCAR Library
P. O. Box 3000
Boulder, Colorado 80302

E&R Center
Bureau of Reclamation
ATTN: D-751, Bldg 67
Denver, Colorado 80225

Armament Dev & Test Center
ADTC (DLOSL)
Eglin AFB, Florida 32542

Commandant
USA Southeastern Signal School
ATTN: ATSO-CTD
Fort Gordon, Georgia 30905

Chief, Technical Services Div
DCS/Aerospace Sciences
ATTN: AWS/DNTI
Scott AFB, Illinois 62225

Commander
US CDC Combat Arms Dev Act
ATTN: ATCACC-CW
Fort Leavenworth, Kansas 66027

Commander
US Army Test & Eval Cmd
ATTN: AMSTE-FA
Aberdeen Proving Ground, MD 21005

Commander
US Army Test & Eval Cmd
ATTN: AMSTE-NBC
Aberdeen Proving Ground, MD 21005

Director
US Army Ballistic Research Lab
ATTN: AMXBR-AM
Aberdeen Proving Ground, MD 21005

Commander
US Army Ballistic Resch Labs
ATTN: AMXBR-IB
Aberdeen Proving Ground, MD 21005

Commander
US Army Ballistic Rsch Labs
ATTN: AMXBR-IC
Aberdeen Proving Ground, MD 21005

Director
USA Ballistic Research Laboratories
ATTN: AMXBR-CA
Aberdeen Proving Ground, MD 21005

Commander
US Army Armament Command
ATTN: SAREA-DE-N, C. G. Whitacre
Aberdeen Proving Ground, MD 21010

Commander
Aberdeen Proving Ground
ATTN: STEAP-TL (Bldg 305)
Aberdeen Proving Ground, MD 21005

NASA Scientific & Tech Info Fac
ATTN: Acquisitions Br
P. O. Box 33
College Park, Maryland 20740

Dir of Dev & Engr
Defense Systems Div
ATTN: SAREA-DE-DDR
        H. Tannenbaum
Edgewood Arsenal, APG, MD 21010

Commander
Edgewood Arsenal
ATTN: SAREA-TS-L (Tech Lib)
Edgewood Arsenal, MD 21010

Director National Security Agency
ATTN: TDL
Fort George G. Meade,
Maryland 20755

Technical Processes Br
D823
Room 806, Libraries Div NOAA
8060 13th St
Silver Spring, MD 20910

Commander
US Naval Ordnance Lab
ATTN: Technical Library
White Oak, Silver Spring, MD 20910

HQ, ESD (TRI)
L. G. Hanscom Field
Bedford, Massachusetts 01730

Meteorology Laboratory
AFCL(LYV)
L. G. Hanscom Field
Bedford, Massachusetts 01730

Air Force Cambridge Rsch Labs
ATTN: LCH (A. S. Carten, Jr.)
L. G. Hanscom Field
Bedford, Massachusetts 01730

Air Force Cambridge Rsch Labs
ATTN: LKI
L. G. Hanscom Field
Bedford, Massachusetts 01730

US Army Liaison Office
MIT Bldg 26, Rm 131
77 Massachusetts Ave.
Cambridge, Massachusetts 02139

US Army Liaison Office
MIT-Lincoln Lab, RM A-117
P. O. Box 73
Lexington, Massachusetts 02173

The Environmental Resch Institute of Michigan
ATTN: IRIA Library
P. O. Box 618
Ann Arbor, Michigan 48107

Mr. William A. Main
USDA Forest Service
1407 S. Harrison Road
East Lansing, Michigan 48823

Commander
US Army Tank-Automotive Cmd
ATTN: AMSTA-RHP
Warren, Michigan 48090

Dr. A. D. Belmont
Research Division
P. O. Box 1249
Control Data Corp.
Minneapolis, Minn. 55440

Director
USA Engr Waterways Exper Sta
ATTN: Library Branch
Vicksburg, Mississippi 39180

Director
USAE Waterways Experiment Station
ATTN: Mr. A. N. Williamson
P. O. Box 631
Vicksburg, Mississippi 39180

Commander
US Army Cold Regions R&E Lab
ATTN: CRREL-RP
Hanover, New Hampshire 03755

Commanding Officer
Picatinny Arsenal
ATTN: SARPA-TS-S, #59
Dover, NJ 07801

Commander
US Army Satellite Comm Agc
ATTN: AMCPM-SC-3
Fort Monmouth, NJ 07703

Commander
US Army Electronics Command
ATTN: AMSEL-BL-CT-S
Fort Monmouth, NJ 07703

Commander
US Army Electronics Command
ATTN: AMSEL-CT-D
Fort Monmouth, NJ 07703

Commander
US Army Electronics Command
ATTN: AMSEL-GG-TD
Fort Monmouth, NJ 07703

Commander
US Army Electronics Command
ATTN: AMSEL-MS-TI
Fort Monmouth, NJ 07703

Commander/Director
US Army Electronics Command
ATTN: AMSEL-NL-D
Fort Monmouth, NJ 07703

Commander
US Army Electronics Command
ATTN: AMSEL-NL-H (EVANS AREA)
Fort Monmouth, NJ 07703

Commander
US Army Electronics Command
ATTN: AMSEL-RD-D
Fort Monmouth, NJ 07703

Mr. Edward C. Nell
US Army Electronics Command
ATTN: AMSEL-SI-CB
Fort Monmouth, NJ 07703

Director, Electronics Technology and Devices Lab
US Army Electronics Command
ATTN: AMSEL-TL-D, Bldg 2700
Fort Monmouth, NJ 07703

Commander
US Army Electronics Command
ATTN: AMSEL-VL-D
Fort Monmouth, NJ 07703

Commander
US Army Electronics Command
ATTN: AMSEL-WL-DI
Fort Monmouth, NJ 07703

Air Force Weapons Lab
ATTN: Technical Library (SUL)
Kirtland AFB, NM 87117

Commander
White Sands Missile Range
ATTN: Technical Library
White Sands Missile Range,
New Mexico 88002

CO, US Army Tropic Test Center
ATTN: STETC-MO-A (Tech Lib)
APO New York 09827

Rome Air Development Center
ATTN: Documents Library
TILD (Bette Smith)
Griffiss Air Force Base,
New York 13440

US Army Rsch, Off. Durham
Box CM, Duke Station
ATTN: CRDARD-IP
Durham, North Carolina 27706

Environmental Protection Agency
Meteorology Laboratory
Research Triangle Park,
North Carolina 27711

Commandant
US Army Field Artillery School
ATTN: ATSF-CTD-A
Fort Sill, Oklahoma 73503

Commandant
US Army Field Artillery School
ATTN: Met Division
Fort Sill, Oklahoma 73503

President
US Army Field Artillery Board
Fort Sill, Oklahoma 73503

Field Artillery Consultants
1112 Becontree Drive
ATTN: ` COL Buntyn
Lawton, Oklahoma 73501

Air Force Avionics Lab
ATTN: AFAL/TSR
Wright-Patterson AFB, Ohio 45433

Commander
Frankford Arsenal
ATTN: Library, K2400, Bldg 51-2
Philadelphia, PA 19137

Commander
Frankford Arsenal
ATTN: SARFA-FCD-O, Bldg 201-2
Bridge & Tarcony Sts.
Philadelphia, PA 19137

Commander
Frankford Arsenal
ATTN: W1000-65-1
Philadelphia, PA 19137

Commander
US Army Nuclear Agency
Building 12
Fort Bliss, Texas 79916

Commander
US Army Air Defense School
ATTN: C&S Dept, MSLSCI Div
Fort Bliss, Texas 79916

Commander
US Army Dugway Proving Ground
ATTN: STEPD-AD-L (Tech Library)
Building 5330
Dugway, Utah 84022

Commander
US Army Dugway Proving Ground
ATTN: TO-M
Dugway, Utah 84022

Mr. Frank D. Eaton
Department of Soil Science and Biometeorology
Utah State University
Logan, Utah 84322

Commander
US Army Materiel Command
ATTN: AMCRD-OS (Mr. Andrew)
Alexandria, Virginia 22304

Mr. Frederick L. Horning
5001 Eisenhower Avenue
ATTN: AMCRD-TV
Alexandria, Virginia 22304

Commander
USA Security Agency Combat Dev Actv
Arlington Hall Station, Bldg 420
Arlington, Virginia 22030

Commander
US Army Security Agency
ATTN: IARD-T
Arlington Hall Station
Arlington, Virginia 22030

CO, USA Foreign Sci & Tech Center
ATTN: AMXST-ISI
220 7th Street, NE
Charlottesville, Virginia 22901

Commander
US Army Engineer Topographic Lab
(STINFO CENTER)
Fort Belvoir, Virginia 22060

Commander
Eustis Directorate
US Army Air Mobility R&D Lab
ATTN: Technical Library
Fort Eustis, Virginia 23604

Commander
US Army Combat Dev Cmd
ATTN: ATCD-CI-I
Fort Monroe, Virginia 23651

Commander
HQ US Army Training & Doctrine Cmd
ATTN: ATCD-FA
Fort Monroe, Virginia 23651

Marine Corps Dev & Educ Cmd
Development Center
ATTN: Cmd, Control, & Comm Div (C³)
Hochmuth Hall
Quantico, Virginia 22134

Commander
US Army Arctic Test Center
ATTN: STEAC-PL-TS
APO Seattle 98733

Director, Systems R&D Service
Federal Aviation Administration
ATTN: ARD-54
2100 Second Street, S.W.
Washington, DC 20590

Chief, Weather Climate
NASA Headquarters
ATTN: Code ERM
Washington, DC 20546

Director
Naval Research Laboratory
CODE 2627
Washington, DC 20375

Dir, US Naval Research Lab
ATTN: Code 5530
Washington, DC 20375

Commander
Naval Elect Sys Cmd HQ
ATTN: CODE 51014
Washington, DC 20360

The Library of Congress
ATTN: Exchange & Gift Div
Washington, DC 20540

Commanding Officer
Harry Diamond Laboratory
ATTN: Library
Washington, DC 20438

National Weather Service
National Meteorological Center
World Weather Bldg - 5200 Auth Rd
ATTN: Mr. Quiroz
Washington, DC 20233

Director
Defense Nuclear Agency
ATTN: Tech Library
Washington, DC 20305

David H. Slade
Leader, Physical and Chemical Transport Pgrm
Division of Biomedical and Environmental Rsch
ATTN: US Atomic Energy Commission
Washington, DC 20545

Commander
Naval Air Systems Command
Meteorological Division
AIR-540
Washington, DC 20360

Commander
Naval Weather Service Command
Washington Navy Yard
Bldg 200, Code 304
Washington, DC 20374

Commander, Naval Ship Systems Cmd
Technical Library, Rm 3 S-08
National Center No. 3
Washington, DC 20360

Dr. John L. Walsh
Code 5503
Navy Research Lab
Washington, DC 20375

Head, Atmospheric Sci Section
National Science Foundation
1800 G. Street, N.W.
Washington, DC 20550

Head, Met Rsch Branch
Meteorological Division
Naval Air Sys Cmd (AIR-5401)
Washington, DC 20361

HQDA (DAEN-RDM/Dr. de Percin)
FORRESTAL BLDG
Washington, DC 20314

Ofc Asst. Sec of the Army
R&D ATTN: Asst. for Rsch
Rm 3-E-379, The Pentagon
Washington, DC 20310

Military Assistant, Environmental Sciences
ODDR&E/E&LS
Pentagon, Room 3D129
Washington, DC 20301

USAFETAC/CB
Navy Yard Annex, Bldg 159
Washington, DC 20333